energies

MDPI

Review

Influence of Water on the Methane Adsorption Capacity of Organic-Rich Shales and Its Controlling Factors: A Review

Yijie Xing [1], Xianming Xiao [1,*], Qin Zhou [2], Wei Liu [1] and Yanming Zhao [1]

[1] School of Energy Resources, China University of Geosciences (Beijing), Beijing 100083, China; 2006210035@email.cugb.edu.cn (Y.X.)
[2] State Key Laboratory of Organic Geochemistry, Guangzhou Institute of Geochemistry, Chinese Academy of Sciences, Guangzhou 510640, China
* Correspondence: xmxiao@cugb.edu.cn

Abstract: A typical feature of shale gas reservoirs is that they contain a significant amount of adsorbed gas. The evaluation and prediction of adsorbed gas play important roles in shale gas exploration and development. However, the presence of water in shale reservoirs makes this work more difficult. In recent years, research related to the occurrence and distribution of water in shales and its effect on methane adsorption have become a prominent issue. In this paper, the factors controlling water in shale nanopores and its influence on methane adsorption were systematically reviewed. It is revealed that the connate water content in shales and their water absorption capacity vary widely, and both are mainly related to the organic matter contents and properties and mineral compositions. The water absorption capacity of organic matter in shales is mainly affected by its nanopore content, structure and surface chemical properties (such as the type and amount of oxygen-containing functional groups), which are jointly constrained by its kerogen type and maturity. Even under moist conditions, the organic matter in shales still shows a strong methane adsorption capacity, although the water decreases the adsorption capacity to some extent. The hydrophilicity of different minerals in shales varies greatly, but the type and amount of clay minerals are the main factors affecting the adsorbed water content or water adsorption capacity of shales. The nanopore structure and characteristics of shales, such as the pore type, specific surface area, pore size distribution and heterogeneity, directly impact the occurrence and distribution of water. The competition for adsorption between water and methane at some adsorption sites is the main mechanism for the reduction in the methane adsorption capacity of moist shales. In addition, external environmental factors, such as pressure and temperature, can change the distribution and occurrence of water in shales and, thus, the influence of water on the methane adsorption capacity to a certain extent. This paper also discusses some current issues regarding the effect of water on methane adsorption capacity and highlights future research directions in this field.

Keywords: shale; nanopore; water adsorption; methane adsorption; controlling factor

Citation: Xing, Y.; Xiao, X.; Zhou, Q.; Liu, W.; Zhao, Y. Influence of Water on the Methane Adsorption Capacity of Organic-Rich Shales and Its Controlling Factors: A Review. *Energies* **2023**, *16*, 3305. https://doi.org/10.3390/en16083305

Academic Editors: Dameng Liu and Reza Rezaee

Received: 24 February 2023
Revised: 26 March 2023
Accepted: 4 April 2023
Published: 7 April 2023

1. Introduction

With the increasing demand for energy and the rapid exploitation of conventional oil and gas resources, unconventional oil and gas resources have gradually become important supplements. Shale gas, as an unconventional natural gas, has attracted attention across the world due to its great resource potential. The geological study of shale gas formation and enrichment has been one of the main research directions of the last 15 years [1–4]. Shale gas occurs mainly in a free state in the pores and fractures of shales and in an absorbed state on the pore surfaces of organic and inorganic components, with a minor amount dissolved in water, oil and bitumen [5–8]. Nanopores are widely developed in shale gas reservoirs, providing them with a large specific surface area and a high proportion of adsorbed gas, making them different from conventional tight gas reservoirs [9–13]. The

adsorbed gas content in shale reservoirs varies greatly, generally accounting for 20–85% of the total gas content [14–21]. Evidently, it is of great significance for shale gas evaluation, exploration and development to understand the methane adsorption capacity of shales and its restrictive factors.

In order to reveal the methane adsorption capacity of shales and evaluate their adsorbed gas contents under geological conditions, the high-pressure methane adsorption experiment is widely applied to simulate methane adsorption, which is usually based on dried shale samples [22–24]. However, there is a more or less certain amount of water in shale reservoirs under geological conditions [25–29]. Water in shales not only reduces the content of free gas but also has a clear influence on the adsorbed gas owing to the competition for adsorption between water and methane in the nanopores [30–32]. With the wide-scale exploration and development of shale gas in recent years, the occurrence and distribution of water in shales, its effect on methane adsorption and its restrictive factors have received extensive attention, and the amount of related research has continuously increased [9,33–40].

The water in a shale reservoir mainly has the following origins: water remaining from sedimentation, water generated by organic matter evolution and mineral diagenesis and water seeping into the reservoir from the surrounding formations. Some studies refer to this water as connate water, with the purpose of distinguishing it from the enthetic water introduced into shale reservoirs through artificial interventions (e.g., drilling and fracturing) [41–45]. Connate water is the research target for the evaluation of shale gas reservoirs. According to the occurrence state of water in shales, it is divided into free water, adsorbed water (also called as irreducible water in some studies) and structured water [46–48]. Among them, adsorbed water has a direct effect on the adsorption of gas in shales [49–51]. A large number of studies have shown that water in gas-bearing shales is generally in a state of ultra-low saturation [27,52–54], and only adsorbed water is present, without free gas [55–57]. It is generally believed that the water in shales reduces their methane adsorption capacity, because the adsorbed water molecules competitively occupy the methane adsorption sites, and the condensate water blocks the micropores and partial pore throats, which prevents methane molecules from reaching some pores [58–61]. However, the study of connate water in shales is challenging, since it is difficult to obtain samples while maintaining the original water-bearing state of shale reservoirs [40,53,62–65]. According to the data obtained by Handwerger et al. (2011), the adsorbed water content of shale samples that were kept in closed bags and stored in room conditions for two years showed no significant change, which means that it is possible to investigate the characteristics of connate water in gas-bearing shales [63]. In recent years, a variety of methods have been developed to study the water in shales. The simulation test methods for obtaining shale samples with water mainly include the following: water displacement [48,66], water spontaneous imbibition [29,67] and equilibrium moisture adsorption [9,28,68–71]. Among them, the water adsorption capacity of shales is generally tested using the equilibrium moisture adsorption experiment method recommended by ASTM (2007) (the achieved water is called equilibrium adsorbed moisture in order to distinguish it from connate water [68]. This method can also be used to obtain shale samples with different moisture contents [72–75]. The quantitative analysis methods for water in shales mainly include the following: heating mass loss [76,77], differential thermal analysis [78] and nuclear magnetic resonance [79,80]. In particular, the low-pressure gas (CO_2 and N_2) adsorption method has been used to reveal the distribution of water in the nanopores of shales in a comparison between the dry shale and its moist sample [37,75,81,82]. Through the improvement of the high-pressure methane adsorption experiment procedure, this technique has been applied to the quantitative evaluation of the methane adsorption capacity of water-bearing shale samples [35,39,69,83]. The comprehensive application of these methods can effectively reveal the water absorption capacity of shales, the occurrence and distribution characteristics of the adsorbed water and the influence of adsorbed water on the methane absorption capacity, and some progress has been made in regard to these areas.

To provide a summary of the influence of adsorbed water on shales' methane adsorption capacity using data from the literature, this paper focuses on the influences of organic matter properties, inorganic mineral compositions and temperature and pressure conditions on the adsorption of water and methane. The purpose is to clarify the mechanism of the influence of water in shales on methane adsorption and provide a scientific basis for the objective evaluation and prediction of adsorbed gas in shale reservoirs and theoretical guidance for shale gas exploration and development.

2. Influence of Water on Methane Adsorption Capacity

There are a number of studies which report on the equilibrium moisture content and methane adsorption capacity of shales [5,9,28,84–89]. Figure 1 presents data on the relationship between the equilibrium moisture content and methane adsorption capacity of shales from some relevant studies. Although these data refer to different shales, and the test temperatures are slightly different, they show a uniform trend. With an increasing amount of water uptake in shales, the methane adsorption capacity decreases, but this negative correlation is not a simple linearity. Roughly speaking, when the moisture content is less than 1% (mass ratio, the same below), the methane adsorption capacity decreases rapidly with the increase in the moisture content; when the moisture content is between 1% and 3%, the methane adsorption capacity decreases significantly with the increase in the moisture content; and when the moisture content is more than 3%, the methane adsorption capacity shows only a slow decrease with the further increase in the moisture content. A similar trend was revealed in some earlier studies. For instance, Crosdale (2008) studied the methane adsorption of sub-bituminous coal samples containing equilibrium moisture (the Huntly coalfield, New Zealand), and his data show that there is a nonlinear negative correlation between the methane adsorption capacity and moisture content [90]. Yang et al. (2016b) reported experimental results on the methane adsorption of overmature shale samples containing different amounts of equilibrium moisture (the Wufeng-Longmaxi Formation, Sichuan Basin, China) and found that with the increase in the moisture content, the methane adsorption capacity presented an initial decline, followed by a steep decline and then a slow decline [91]. In fact, there is a critical moisture content for the effect of water on methane adsorption in shales [9,22,28,88,92]. When the moisture content is less than this value, the methane adsorption capacity decreases significantly with the increase in the moisture content, while the decrease in the methane adsorption capacity becomes rather slow with the further increase in the moisture content when it exceeds this value. It can also be seen from Figure 1 that the critical moisture content is variable between different shales, with an approximate range of 1.5–3.5%. Sun et al. (2021b) reported the relationship between the GIP (gas in place) content (66–93% adsorbed gas) and water saturation of shallow Longmaxi shale from the Xishui Block, Guizhou, China, and it is similar to the trend presented in Figure 1. With the increase in water saturation, the GIP content decreases first rapidly and then slowly, and even if the water saturation reaches a high level (60–80%), there is still a certain amount of gas (mainly adsorbed gas) stored in the shale [93]. This shows that the critical moisture content of shales can also be reached under geological conditions. The available data have shown that the critical moisture content of a specific shale is mainly controlled by its geochemical attributes and nanopore characteristics [40,94,95]. However, systematic research on this aspect is still lacking, and a further work is needed.

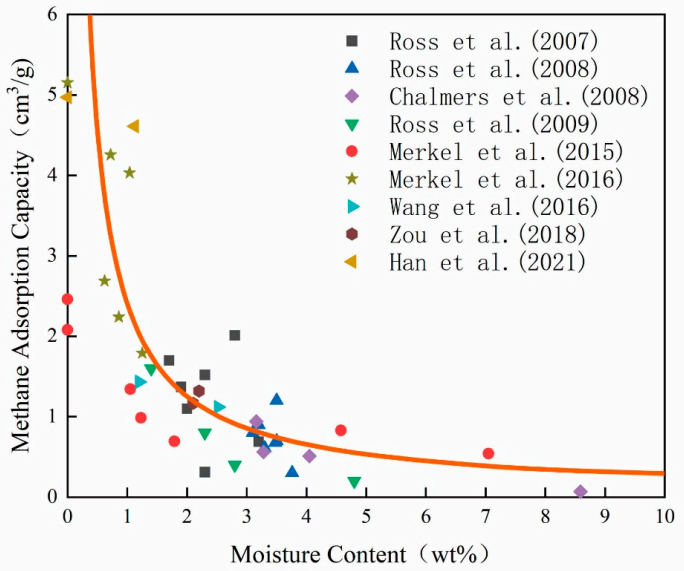

Figure 1. Relationship between equilibrium moisture content and methane absolute adsorption capacity of shales (pressure 6 Mpa, temperature 298–318 K). The data sources are as follows: the Gordondale and Muskwa shales in British Columbia, Canada [5,85]; the Lower Cretaceous shale in northeastern British Columbia, Canada [33]; the D-M shale in British Columbia, Canada [9]; the Bossier, Haynesville, in Texas and Louisiana, USA, and the LOS shales in the Midland Valley Basin, Scotland [28,87]; the Carboniferous Keluke Formation shale in the eastern part of Qaidam Basin, China [88]; the Carynginia Formation shale in the Perth Basin, Western Australia [89]; the Longmaxi shale in the southeastern part of Sichuan Basin, China [96].

Methane adsorption on shale nanopore surfaces is regarded as physisorption through Van der Waals force, while water adsorption is a combination of physisorption and chemisorption, i.e., van der Waals force combined with adhered force from the polar bonds of water molecules [97]. When water enters into shale nanopores, if the force between the water molecules and pore surfaces is greater than that between the methane and pore surfaces, the adsorbed methane will be replaced with water [98]. Therefore, it is generally believed that the water in shales reduces their methane adsorption capacity, because the adsorbed water molecules competitively occupy the methane adsorption sites, and/or the condensate water blocks the micropores and partial pore throats, which prevents methane molecules from reaching these pores [58–61]. The dynamic behavior of water in shale nanopores is related to its amount, which leads to differences in the reduction extent of the methane adsorption capacity under different moisture content conditions. Because the adsorption of water and methane in shales basically occurs in the nanopores of organic matter and clay minerals [11,99–102], the occurrence and distribution of water in the pores have been highlighted. Chalmers and Bustin (2008) investigated the methane adsorption capacity of shale samples with equilibrium moisture (the Lower Cretaceous shale, northeastern British Columbia, Canada) and found that some of the samples with a high moisture content also had a high methane adsorption capacity, and they believed that was because the adsorption sites of the water and methane were different, and the hydrophobic sites of organic matter could adsorb a certain amount of methane even at a high moisture content [33]. Li et al. (2016) studied the interaction between methane, water films and clay minerals in shales and argued that when the water coverage rate on the surfaces of clay minerals exceeded the monolayer level, a transition from a gas–solid boundary adsorption to a gas–liquid interface adsorption occurred, but when the water coverage rate was less than the monolayer level, there was competition for adsorption sites between the water and methane [31]. Zou et al. (2018) compared the methane adsorption capacities of dry shales and samples of those shales containing equilibrium moisture (the Perth Basin, Western Australia) and highlighted that water existed on the clay surface in

the form of a water film, which changed the interface interaction between the methane and clay [89]. Li (2019) also considered that the change in the adsorption interface caused by the increase in the moisture content was the main mechanism for the decrease in the methane adsorption capacity [103].

Under different moisture content conditions, the occurrence and distribution characteristics of water in shale nanopores also differ to some extent (Figure 2) [96,104,105]. When the moisture content is low, the water molecules firstly combine with hydrophilic oxygen-containing functional groups in organic pores and enter inorganic mineral pores with the reduction in the number of methane adsorption sites [106]. At the hydrophobic point, organic pores adsorb almost no water molecules, while water is adsorbed by the clay pores in a monolayer and engages in competitive adsorption with methane (Figure 2a). This results in a rapid decrease in the methane adsorption capacity. As the moisture content continues to increase, water tends to accumulate at the pore center, which prevents the flow of methane molecules into narrow pores. When the moisture content reaches a certain level, the water in the organic pores forms capillary water, while the water in the clay mineral pores undergoes multilayer adsorption [107,108], and the water film at the pore throats accumulates into a water bridge and gradually forms capillary water to prevent methane from flowing into the relevant pores, thus decreasing the diffusion and adsorption capacity of methane in the pores of clay minerals (Figure 2b). When the moisture content reaches a high level, the water in organic pores will form a highly ordered structure (water clusters) [105], and the water bridge in the clay pores will gradually form condensate water with the increase in the amount of capillary water (Figure 2c). Under this condition, the influence of water on methane adsorption basically reaches a limit, and even if the moisture content continues to increase, its effect on the methane adsorption of shales will not be significant.

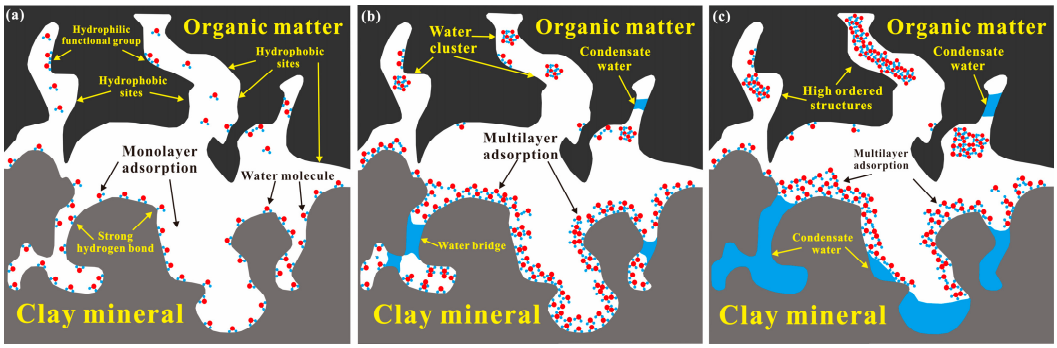

Figure 2. Occurrence and distribution characteristics of water in shale under different moisture content conditions. (**a**) Low moisture content. (**b**) Moderate moisture content. (**c**) High moisture content. These figures are modified from Han et al. (2021) [96].

Therefore, the adsorption of water on the pore surfaces of shales can be divided into monolayer adsorption, multi-layer adsorption and capillary condensation. These three different forms of adsorbed water are controlled by the amount of water, which is responsible for the three stages forming the relationship between methane adsorption and the moisture content described above. It can also be seen from Figure 1 that, for a given equilibrium moisture content, the different shales have variable methane adsorption capacities.

The effect of water on the methane adsorption of shales depends on the amount of water and the occurrence and distribution of water in the nanopores. These two aspects are related to the geochemical attributes of shales (such as the organic matter content, type and maturity and the mineral composition, especially the type and amount of clay minerals) and their nanopore development characteristics (such as the pore type, pore structure, pore size distribution and pore heterogeneity). In addition, some geological conditions (such as temperature and pressure) of shale reservoirs also alter the influence of water on methane adsorption. These processes are summarized below.

3. Effects of Organic Matter Attributes on the Adsorption of Water and Methane

There is a process for understanding whether there is a significant amount of water in the organic pores of shale gas reservoirs. Earlier studies posited that the hydrophobic surface of organic matter in shales is not conducive to the occurrence of water, and there is almost no water in organic pores [54,109–111]. Water mainly exists in inorganic pores, especially in the nanopores of clay minerals with strong hydrophilicity [44,72,112–116]. However, for low- and middle-mature shales, a certain amount of hydrophilic functional groups are present in their organic matter molecular structure, and water can be combined with the polar oxygen-containing functional groups of organic matter through hydrogen bonding; thus, water may be present in organic pores [117–119]. In particular, recent studies have shown that the polar oxygen-containing functional groups of organic matter in shales are basically shed in the high- and over-mature stages, but the organic nanopores can still capture a small amount of water through capillary forces [57,64,120–122]. In fact, the capacity of organic pores in shales to absorb a certain amount of water is not only restricted by the surface wettability but also related to the pore structure characteristics, which are mainly controlled by the amount, type and maturity of organic matter [119,123].

3.1. Total Organic Carbon Content

Figure 3a,b presents data on the total organic carbon (TOC), equilibrium moisture and connate water contents of high- and over-mature shales reported in the literature. With the increase in the TOC content, both the equilibrium moisture and connate water contents lack a uniform change trend. In fact, the correlations between the TOC and equilibrium moisture (or connate water) contents of shale samples from different basins or different areas are also significantly different. For example, according to the data for the Lower Cretaceous low-middle-mature shale in northeastern British Columbia, Canada, reported by Chalmers and Bustin (2008), there was no clear correlation between the TOC and equilibrium moisture contents, and the authors believed that the reason for this was the effect of a high content of clay minerals in this shale [33]. The data provided by Cheng et al. (2017) on high- and over-mature shales from southern China indicate that the connate water content has a clear positive correlation with the TOC content [64]. Results similar to those of Cheng et al. (2017) were also derived from shales in other basins (e.g., [75,84,89,124]). Sun et al. (2020) conducted a study of the connate water of over-mature Longmaxi shale from northern Guizhou, China, and their data show that the TOC content is negatively correlated with the water content, while the clay mineral content is positively correlated with the water content. The authors believed that the water mainly existed in clay mineral pores, and the negative correlation between the TOC and water content was caused by the negative correlation between the TOC and clay minerals [125]. In order to eliminate the influence of clay minerals in shales, the equilibrium moisture content of Lower Jurassic low-middle-mature shale (British Columbia, Canada) reported by Ross and Bustin (2007) was normalized to the clay mineral content (the ratio of moisture content to clay mineral content), and the results showed that the normalized moisture content had a positive correlation with the TOC content (Figure 3c) [5]. Cheng et al. (2022) selected a set of over-mature coal-measure shales (the Qinshui Basin, North China) with similar clay mineral contents (33.2–36.4%) and variable TOC contents to investigate the occurrence characteristics of the connate water and equilibrium moisture and found that both had a strong, positive correlation with the TOC content (Figure 3d) [65].

It can be seen from the above discussion that although the water adsorption capacity or connate water content of shales is mainly controlled by the clay minerals, a small amount of water can still be adsorbed in the organic nanopores. This mechanism is generally explained by hydrogen bond binding between the water and hydrophilic oxygen-containing functional groups in organic matter or the capillary force effect of water in organic nanopores [118,126–128].

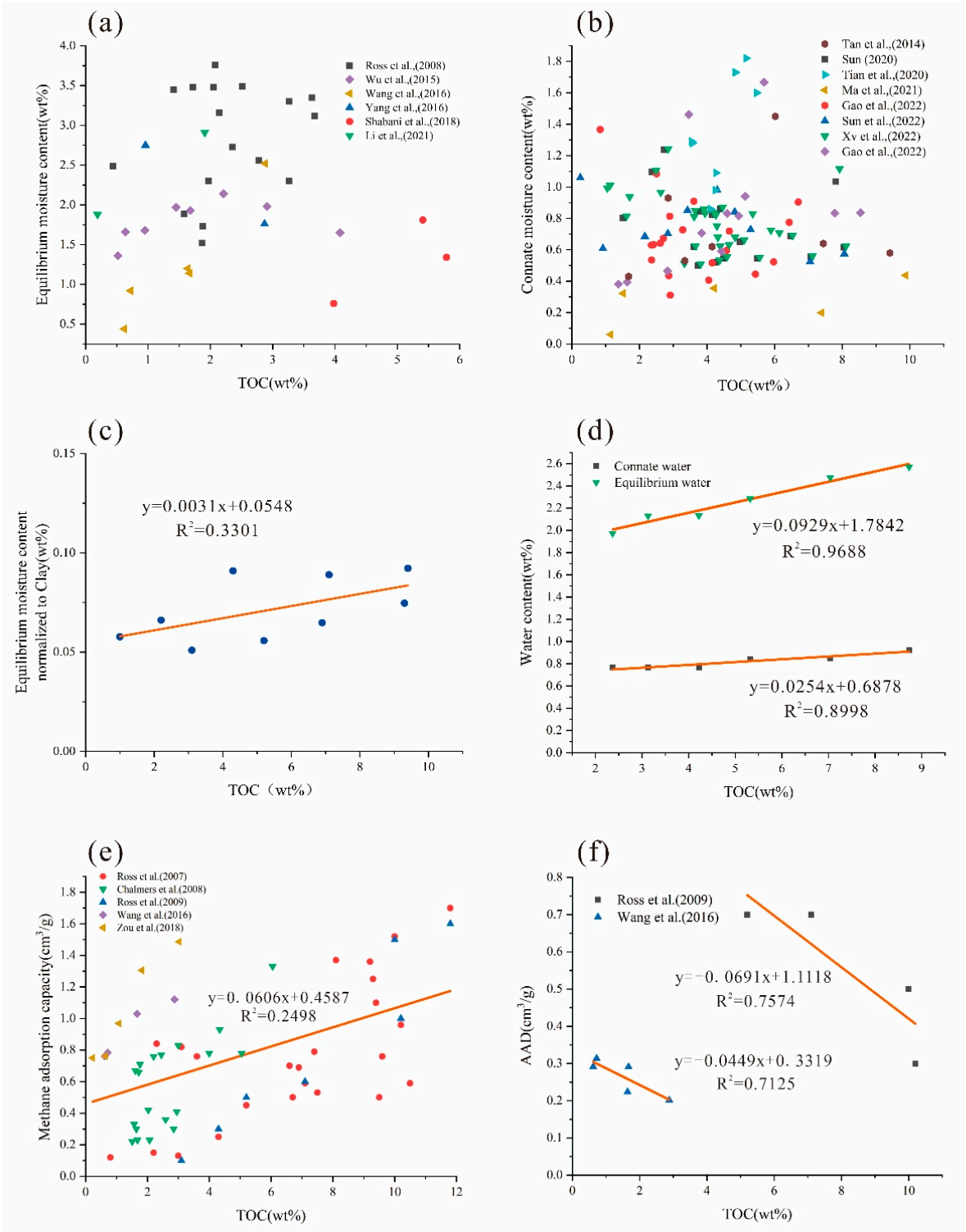

Figure 3. Relationships of TOC content with equilibrium moisture content, connate water content, methane adsorption capacity, and methane adsorption capacity differences between dry and moist conditions in shales. (**a**) TOC content versus equilibrium moisture content (Ro between 1.25% and 3.6%). The data of Ross and Bustin (2008) are derived from the Muskwa shale in the northwestern region of the Western Canada sedimentary basin [85]. The data of Wu et al. (2015) are derived from the Longmaxi Formation shale from the XY1 well in Guizhou and the outcrops of Fenghuang and Yongshun in Hunan, China [129]. The data of Wang and Yu (2016) are derived from the Carboniferous Keluke Formation shale from the CY2 well in the Qaidam Basin, China [88]. The data of Yang et al. (2016b) are

derived from the Wufeng-Longmaxi Formation shale in the Sichuan Basin, China [91]. The data of Shabani et al. (2018) are derived from the Sargelu-Garau Formation shale in southwestern Iran [130]. The data of Li et al. (2021b) are derived from the Shanxi-Taiyuan Formation shale in the North China Basin, China [73]. (**b**) The correlation between the TOC content versus connate water content (Ro between 2.4% and 3.6%). The data of Tan et al. (2014) are derived from the Lower Cambrian and Lower Silurian shale in the Upper Yangtze region of South China [131]. The data of Sun (2020) are derived from shale of the shallow Longmaxi Formation in the Qianbei area, Sichuan Basin, China [125]. The data of Tian et al. (2020) are derived from shale of the Lower Cambrian Qiongzhusi Formation, Upper Ordovician Wufeng Formation and Lower Silurian Longmaxi Formation, Sichuan Basin, China [71]. The data of Ma et al. (2021) are derived from the coal-measure shale of the Taiyuan Formation in the Yushe area, Qinshui Basin, China [132]. The data of Gao et al. (2022a) are derived from the deep Lower Cambrian Longmaxi Formation shale in the Luzhou block, southern Sichuan, China [75]. The data of Sun et al. (2022) are derived from the carboniferous coal-measure shale in the Yangquan block, Qinshui Basin, China [39]. The data of Xu et al. (2022) are derived from Lower Silurian Longmaxi Formation shale and Lower Cambrian Niutitang Formation shale in southeast Chongqing, China [40]. The data of Gao et al. (2022b) are derived from ultra-deep shale of the Lower Paleozoic Wufeng-Longmaxi Formation in the eastern part of Sichuan Basin, China [133]. (**c**) Correlation between equilibrium moisture content normalized to clay mineral content and TOC content (Ro between 0.56% and 1.16%). The Lower Jurassic Gordondale and Poker shale from northeastern British Columbia, Canada. The data are derived from [5]. (**d**) Correlation between TOC content and moisture content (Ro between 3.4% and 3.6%). The Lower Permian Shanxi Formation and Upper Carboniferous Taiyuan Formation shales of the Yangquan block, Qinshui Basin, China. The data are derived from [65]. (**e**) Correlation between TOC content and methane adsorption capacity of shale containing equilibrium moisture (Ro between 0.6% and1.59%, pressure 6MPa, temperature 298–319.15 K). The data of Ross and Bustin (2007) are derived from the Lower Jurassic Gordondale and Poker chip shales in northeastern British Columbia, Canada [5]. The data of Chalmers and Bustin (2008) are derived from Lower Cretaceous shales in northeastern British Columbia, Canada [33]. The data of Ross and Marc Bustin (2009) are derived from the Jurassic shales in British Columbia, Western Canada [9]. The data of Wang and Yu (2016) are derived from the CY2 well shale of the Carboniferous Keluke Formation in the eastern part of Qaidam Basin, China [88]. The data of Zou et al. (2018) are derived from the AC2 well shale of the Carynginia Formation in Perth Basin, Western Australia [89]. (**f**) Correlation between TOC content and AAD (pressure 6 MPa, temperature 298–319.1 5 K). The data of Ross and Marc Bustin (2009) are derived from the Jurassic shale in British Columbia, Western Canada (Ro between 0.9% and 1.3%) [9]. The data of Wang and Yu (2016) are derived from Carboniferous Keluke Formation shale from the CY2 well in the eastern part of Qaidam Basin, China (Ro between 1.35% and 1.69%) [88].

For shale samples containing equilibrium moisture, the methane adsorption capacity has a clear positive correlation with the TOC content (Figure 3e), indicating that organic matter still has a strong methane adsorption capacity under moist conditions and controls the methane adsorption capacity. Figure 3f shows the correlation between the TOC content and AAD (the difference in the methane adsorption capacity of shales under dry and equilibrium moisture conditions) based on the data reported by Ross and Bustin (2009) and Wang and Yu (2016) [9,88]. Although the two sets of shales originate from different basins, their AAD results show a decreasing trend with the increase in the TOC content. This further shows that the influence of water on methane adsorption will decrease with the increase in the TOC content. The same conclusion can be derived from the data reported by other authors (e.g., [91,130]). Relevant mechanism explanations have also been proposed [30,134–137]. For example, Tong et al. (2011) and Wei et al. (2014) believed that in shales with higher TOC contents, the organic matter has a better interconnected pore system and more hydrophobic sites than minerals with a stronger pore water preservation capacity, and moreover, the limited hydrophilic sites in the organic matter can only form a small number of water clusters, which is conducive not to the adsorption of water but to the transport of water, thus reducing the influence of water on methane adsorption, com-

pared with shales with lower TOC contents [134,136]. Billemont et al. (2013) investigated the adsorption of methane in nanoporous carbon with adsorbed water using molecular simulations. Their results show that in the competitive adsorption process between water and methane, the water in organic pores has a trend of desorption with the increase in methane pressure, which implies that the influence of water on methane adsorption in shales with high TOC contents might be mitigated [135].

3.2. Organic Matter Type

The organic matter in shales is divided into three kerogen types: type I, type II and type III [138,139]. Although the organic matter in coals is generally regarded as typical type III kerogen [140], coals contain most of the macerals occurring in shales. Therefore, the research results on coals can provide some references for shales.

Chalmers and Bustin (2008) studied the methane adsorption capacity of low-middle-mature shales containing equilibrium moisture and found that after the moisture content data was normalized to the TOC, the normalized moisture content of the type III shale samples was higher than those of the type I and type II shale samples [33]. Li (2021) investigated the relationship between the water contact angle and maturity of shales with different kerogen types and found that when Ro < 2.0%, the type III shale had the smallest contact angle, followed by type II and type I shales, but when Ro > 2.0%, the difference in the water contact angle between the three types of shales was not clear (Figure 4a) [141]. This indicates that the hydrophilicity of organic matter decreases successively from type III to type II to type I, and this difference occurs mainly in the maturity range from the immature to middle-mature stages but is not significant in the high- and over-mature stages.

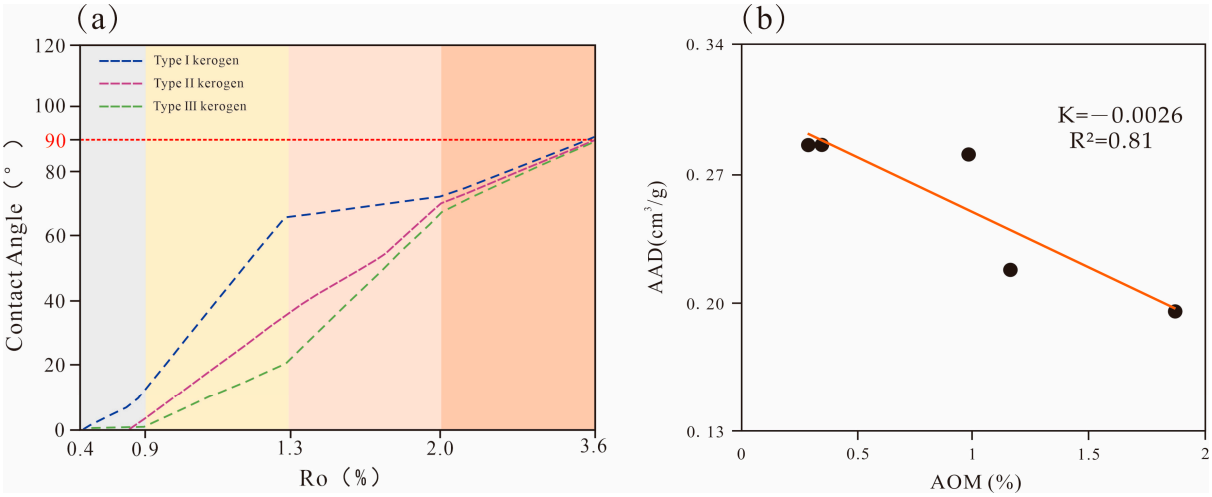

Figure 4. (**a**) Correlation between the water contact angle and maturity of shales with different types of kerogen. A smaller water contact angle indicates a better wettability. The red line is the dividing line between hydrophilic and hydrophobic kerogen. This figure is modified from [141]. (**b**) Correlation between the amorphous organic matter content (AOM) and AAD in shales. This figure is derived from [88].

Hydrophobicity differs considerably between different macerals. Arnold and Aplan (1989) studied the hydrophobicity of different macerals in coals of low-middle maturity using the water contact angle method and obtained the following order of hydrophobicity: exinite > vitrinite > inertinite (Table 1) [142]. Xu et al. (2015) investigated the influences of maceral components on the wettability of water-containing coal samples (Ro = 1.0%) and also found that the coals rich in vitrinite had a strong hydrophilicity, and the authors believed that the high proportion of hydroxyl functional groups on the surface of the vitrinite was an important reason for its strong wettability [143]. Wang and Yu (2016) conducted a comparative study on the methane adsorption capacity of shales (low-middle

maturity) under dry and moist (equilibrium moisture) conditions (the samples were from the Qaidam Basin, China) and found that the dense hydrophobic groups on the surface of amorphous kerogen can "resist" water adsorption. According to their data, when the content of amorphous kerogen in the shales is higher, the methane adsorption is less affected by water, and the difference in methane adsorption capacity (AAD) between dry shales and their moist samples shows a clear, linear, negative correlation with the content of amorphous kerogen, with a correlation coefficient of 0.81 (Figure 4b) [88].

Table 1. Comparison of contact angles of exinite, vitrinite and inertinite in coals (data from [142]).

Sample	Seam Rank	Maceral	Contact Angles θ (°)	Ro (%)
Carbon Co., UT		Liptinites	120	0.5
	subA	Vitrinite	35	0.5
		Fusinite	25	0.5
Parke Co., IN		Liptinites	90	0.6
	hvBb	Vitrinite	57	0.6
		Fusinite	41	0.6

The difference in hydrophilicity between different kerogen types or their macerals is directly related to their chemical structure and is affected by their maturity. Water interacts with different types of functional groups on the surface of organic matter and inside its pores, especially in the low- and middle-mature stages, and thus organic matter can absorb a certain amount of water [37,118,144,145]. The properties of heteratomic functional groups (mainly oxygen-containing functional groups) of organic matter are directly related to its kerogen type [146] (Ungerer, 1990). Type I and type II kerogens mainly contain ether bonds and ester groups, respectively, while type III kerogen mainly consists of phenolic hydroxyl, quinone and aryl carboxyl groups [147]. Joubert et al. (1974) studied the methane adsorption behavior of coals of different maturities under dry and moist conditions and found that the reduction in the methane adsorption capacity of high-oxygen coals (i.e., lower maturity) was much greater than that of low-oxygen coals (higher maturity) when these coals were saturated with water compared with their dry samples. The authors also noted that only the adsorbed water could affect the gas adsorption capacity, while an excessive amount of condensed water had no noticeable effect [49]. Using the Grand Canonical Monte Carlo method and molecular dynamics simulation, Xiang et al. (2014) simulated the interaction between low-mature coal (Ro = 0.62%) and water. The results showed that water mainly forms in a stratified distribution around the hydroxyl, carboxyl and carbonyl groups on the surface of the coal, and the interaction intensity is as follows: hydroxyl group > carboxyl group > carbonyl group [148]. Xia et al. (2016) applied the quantum chemical density functional theory (DFT) to study the adsorption mechanism of water molecules with oxygen-containing functional groups on the surface of a lignite model and achieved results showing that the adsorption order of oxygen-containing functional groups on water molecules is as follows: carboxyl > phenol hydroxyl > alcohol hydroxyl > carbonyl > ether bond (Table 2) [149]. Therefore, the difference in chemical structure between different types of kerogen (typically in the low- and middle-mature stages), especially the difference between oxygen-containing functional groups, is the basic reason for their different hydrophilicities. The water adsorption capacity of type III kerogen is stronger than that of types I and II. Due to the gradual shedding of these functional groups of organic matter in the process of thermal evolution, the ratio of hydrogen to carbon and that oxygen to carbon in organic matter decrease with enhanced aromatization [150,151]. When evolved to the overmature stage, the chemical structure characteristics of different types of kerogen become very similar, and the difference in water adsorption capacity between them is no longer apparent.

Table 2. Adsorption energy of water molecules acting on different oxygen-containing functional groups of a lignite model (data from [149]).

Adsorption Site	* $E_{coal/water}$/(kJ/mol)	* E_{ads}/(kJ/mol)
Carboxyl	7,039,986.00	−69.25
Phenolic hydroxyl	7,039,962.37	−45.63
Alcoholic hydroxyl	7,039,957.81	−41.06
Carbonyl	7,039,953.30	−36.55
Ether linkage	7,039,939.84	−23.10

* $E_{coal/water}$ is the total energy after lignite absorbs the water molecules. E_{coal} and E_{water} are the energies of lignite and water molecules, respectively. E_{ads} is the adsorption energy of water molecules on the surface of lignite. * $E_{ads} = E_{coal/water} - E_{coal} - E_{water}$. A greater absolute value of E_{ads} indicates stronger adsorption, since the adsorption process is exothermic.

Hydrophilicity clearly differs between different types of kerogen in different stages of maturity, which also affects their methane adsorption. Huang et al. (2018a) combined the molecular dynamics and Grand Canonical Monte Carlo methods to simulate the methane adsorption behaviors of different types of immature kerogen models under dry and moist conditions. The results showed that the methane adsorption capacity of type III kerogen was greater than that of type I and type II kerogens when the moisture content was between 0.6% and 2.4%, while compared with the dry samples, the decrease in the methane adsorption capacity of type III kerogen under moist conditions was greater than that of the other two types of kerogen at the same moisture content, a finding which is mainly attributed to the former's higher hydrophilicity [106]. At present, there is no literature on the comparative study of the water adsorption capacities of different types of kerogen in a higher stage of maturity. However, some studies have shown that the functional groups of organic matter in coals and shales are basically eliminated when they evolve into the high- and over-mature stages [146,152,153], and in this case, organic nanopores, especially micropores and smaller mesopores, play a crucial role in water adsorption [121–123]. The developmental degree of organic nanopores of type III kerogen is significantly lower than that of type I and type II kerogens in the high- and over-mature stages [84,154,155], and it is reasonable to infer that type I and type II kerogens have a relatively stronger water adsorption capacity than type III kerogen.

To sum up, the properties and number of functional groups of organic matter in shales are the main factors controlling their hydrophilicity, which is restricted by their maturity. The difference in hydrophilicity between different types of kerogen is clear from the immature to middle mature stages. At present, the adsorption capacities of water and methane have been investigated extensively for specific shales, but research on the water adsorption capacities of shales with different types of kerogen of different maturities and their methane adsorption capacities under moist conditions is still lacking, and systematic, comparative research is needed.

3.3. Maturity of Organic Matter

There are some relevant studies on the correlation between the maturity, moisture content and methane adsorption capacity of shales, which confirm that the amount of connate water in shales is controlled by their maturity, and maturity also affects the adsorption capacity of shales for water and methane.

In order to understand the evolution of connate water in shales during thermal maturation and avoid the influences of various uncertain factors under geological conditions, Cheng et al. (2019) conducted a thermal simulation experiment to investigate the change in water content of an organic-rich shale containing type II kerogen with increasing maturity. The results showed that the water content decreased significantly when Ro increased from 0.67% to 0.90%, increased rapidly when Ro increased from 0.90% to 1.36%, decreased observably when Ro increased from 1.36% to 1.90% and then decreased slowly when Ro > 1.9%. The shale still had a water content of 0.97% as it evolved to a very high stage of maturity (Ro = 3.2%) (Figure 5) [156]. The above evolutionary process roughly corresponds

to the four stages (oil window, condensate, wet gas and dry gas) of oil and gas generation from source rocks. Although the change in the water content of shales is mainly controlled by the intensity of hydrocarbon generation and expulsion [52,56,157,158], the amount of water generated by the decomposition of clay minerals (i.e., autogenous water) also has a clear effect [43,159–161]. In the oil window stage, the decrease in the water content is mainly due to the displacement of liquid hydrocarbon, which promotes the expulsion of water [162]. In the condensate stage, the transformation of clay minerals generates a certain amount of water, which leads to an increase in the water content [159,161,163]. In the wet gas stage, the transformation of clay minerals is basically completed, the hydrophilic functional groups of organic matter are significantly degraded, and the clear decrease in the amount of water is due to the displacement of gaseous hydrocarbons and their expulsion with the water. In the dry gas stage, gas generation due to heavy hydrocarbon gas secondary cracking and kerogen cracking causes water evaporation and expulsion, which further reduces the water content, but the clay minerals and widely developed organic nanopores can still retain a certain amount of water. This simulation experiment result is consistent with the occurrence characteristics of connate water in shale gas reservoirs under geological conditions. For example, the Longmaxi Formation over-mature gas shale samples from a well in the northern area of Guizhou, China, have an average connate water content of 7.46 mg/g, and the water occupies 82% and 41% of the inorganic and organic non-micropore BET surface areas, respectively, and 44% and 18% of the inorganic and organic micropore volumes, respectively [93].

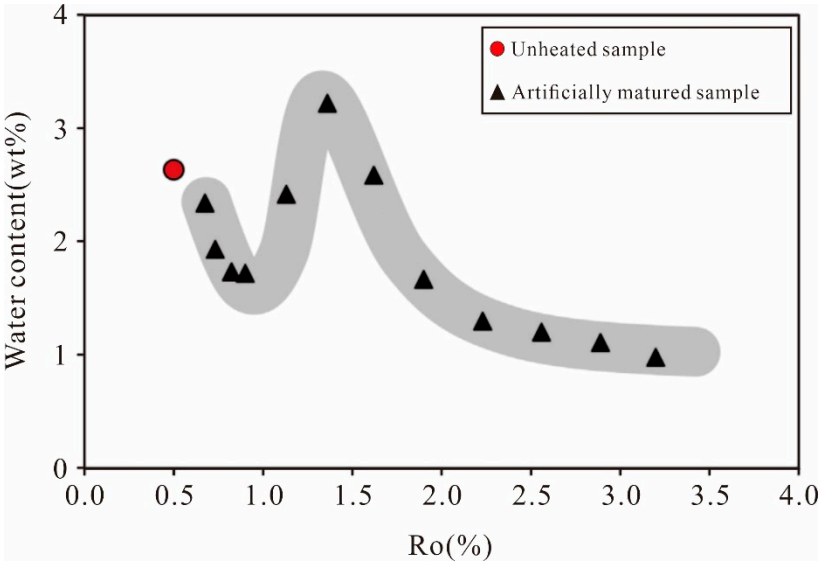

Figure 5. Correlation between the maturity and water content of an organic-rich shale. The data are based on a thermal simulation experiment of this shale [156].

In fact, the thermal maturation of organic matter is also accompanied by the evolution of its water absorption ability (i.e., hydrophilicity), which impacts the amount of connate water in shales [119,164–166]. Hu et al. (2016) used the molecular dynamics simulation method to study the influence of maturity on the wettability of an organic pore system and indicated that the wettability of kerogen was a function of its maturity. It was hydrophilic even in a very low stage of maturity, seemed to exhibit mixed (oil and water) wettability in the middle-mature stage, and exhibited oil wettability in the high-mature stage [119]. Jagadisan and Heidari (2019) studied the wettability of a set of kerogen samples of different maturities obtained by heating treatment and found that the kerogen was hydrophilic in low maturity and gradually changed to become lipophilic and hydrophobic in high maturity, and the same rule remained true after the removal of soluble organic matter from the kerogen [165]. The measured data on the electrical resistivity, dielectric constant

and elastic modulus of kerogen samples provided by some authors (e.g., [167–169]) also indirectly indicate that the water adsorption capacity of shales varies according to thermal maturity. As mentioned above, in the stages of low and middle maturity, the influence of maturity on the water adsorption capacity of organic matter is mainly attributed to the continuous shedding of oxygen-containing functional groups with increasing maturity. Guo et al. (2014) conducted systemic research using a carbonaceous shale kerogen which was pyrolyzed at different temperatures and then analyzed by infrared spectroscopy and found that the number of oxygen-containing functional groups decreased sharply with the increase in maturity and basically disappeared after the pyrolysis temperature reached 450 °C (Ro = 1.5%) [153]. The molecular simulation results of Hu et al. (2015) show that the water accessibility of nanopores in kerogen depends on the stage of maturity and pore surface roughness, and it is difficult for water to enter organic ultra-micropores (pore size < 0.4 nm) or pores without oxygen functional groups [118].

However, high- and over-mature shales still have the ability to adsorb water, even though their organic matter lacks polar functional groups [118,120–122,170–172], which is mainly attributed to the extensive development of organic nanopores. According to a study conducted by Curtis et al. (2012) on Woodford shale, organic matter begins to develop a large number of nanopores only when its maturity is over 1.23% Ro [173]. The simulation results of Chen and Xiao (2014) show that the nanopore structure parameters of organic matter in shales will increase with increasing maturity until the level of maturity reach about 3.5% [174]. Cao et al. (2015) analyzed the specific surface areas of kerogen samples of different maturities. According to their data, low-mature kerogen has a very low specific surface area (5.54–27.49 m^2/g), while high- and over-mature kerogens have a much greater specific surface area (161.23–300.30 m^2/g) [175]. Chen et al. (2021) studied the water adsorption behavior of high- and over-mature shales of the Wufeng-Longmaxi Formation in the eastern part of Sichuan Basin, China, and its relationship with the pore structure and organic and inorganic components. They highlighted that, compared with inorganic pores, organic pores of the same size have a higher filling pressure, with greater water condensation, and are more likely to dominate water adsorption [172]. A high- or over-mature shale gas reservoir usually shows ultra-low water saturation, and its organic nanopores develop well [57,64,158,176]. According to the Young–Laplace and Kelvin equations, capillary pressure is inversely proportional to water saturation [116], and a high capillary pressure will greatly improve the water-capturing ability. This is the water adsorption mechanism for high- and over-mature shales.

The change in the water adsorption capacity of organic matter during thermal evolution also affects its methane adsorption performance to a certain extent, which depends on the maturity of the organic matter [34,94,177–179]. Gensterblum et al. (2013) reported the methane adsorption capacities of coals of different maturities (from the Ruhr Basin in Germany and the Surat Basin in Australia, with Ro values of 0.5–3.3%) under dry and moist conditions. Their data showed that for the coal samples with similar TOC contents, the difference in the methane adsorption capacity between dry and moist conditions decreased with increasing maturity. The authors believed that this was related to the number of functional groups in these coals [34]. Huang et al. (2018b) studied the effects of maturity (from low maturity to over-maturity) and moisture content on kerogen methane adsorption capacity and behavior based on a real kerogen model. The results showed that, under the condition of a higher moisture content, the reduction in the Langmuir maximum methane adsorption capacity caused by water (LMAC reduction%) decreases with increasing maturity, and this trend can be attributed to the decomposition of hydrophilic groups and the increase in pore size during the maturation of kerogen (Figure 6a) [178]. Sui et al. (2020) applied the Monte Carlo model and molecular dynamics method to simulate the methane adsorption behavior of type II kerogen models of different maturities in the presence and absence of water (II-A, II-B, II-C and II-D correspond to the four stages of low-, middle-, high- and over-mature, respectively). The results showed that under the same water molec-

ular weight conditions, the decrease in the methane adsorption capacity of the kerogen caused by water followed the order of II-A > II-B > II-C > II-D (Figure 6b) [179].

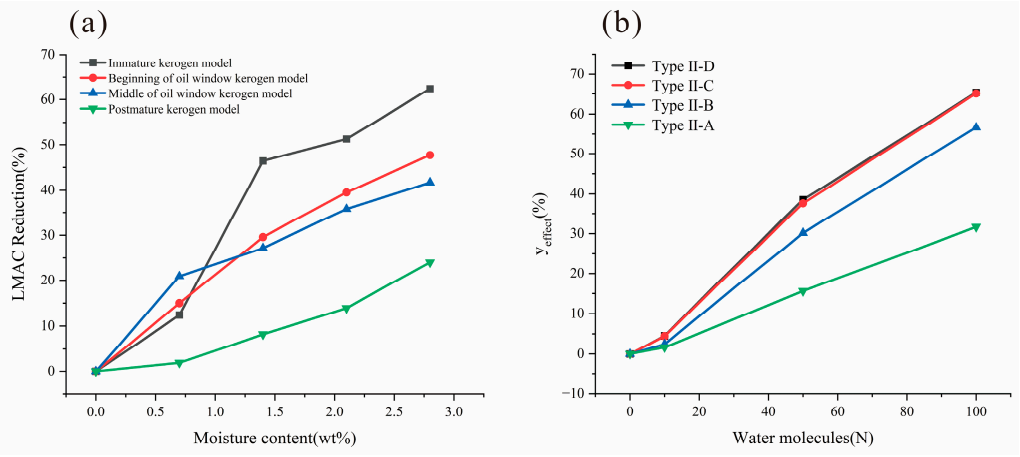

Figure 6. (**a**) The reduction in the Langmuir maximum methane adsorption capacity (LMAC) of kerogen models of different maturities with increasing moisture content. The LMAC reduction is defined as the ratio of reduced LMAC at a certain moisture content to the LMAC under dry conditions. The data are from [178]. (**b**) Degree of influence of water on the methane adsorption capacity under different water molecular weight conditions. y_{effect} = (methane adsorption capacity in the absence of water—methane adsorption capacity in the presence of water)/methane adsorption capacity in the absence of water ×100%. N is the number of water molecules in the kerogen. The four kerogen models (II-A, II-B, II-C and II-D) correspond to the four stages of thermal maturation (low-, middle-, high- and over-mature). The data are from [179].

It can be seen from the abovementioned studies that the occurrence, distribution and mechanism of water in shales change according to their maturity, thus affecting the methane adsorption capacity. Under geological conditions, in order to objectively evaluate the influences of maturity on the adsorbed water and adsorbed gas of shales, it is necessary to comprehensively analyze various correlated factors, such as the TOC content, organic matter type, mineral composition and diagenesis of shales. Compared with low- and middle-mature shales, the water occurrence mechanism in the organic nanopores of high- and over-mature shales is still unclear. It is worth mentioning the work of Kozbial et al. (2014), who found that the basal surface of highly ordered pyrolytic graphite is hydrophilic [170]. Does this mean that the relative hydrophobicity of organic matter pores will change in a very high stage of maturity? All these problems need to be explored further.

4. Effect of Mineral Composition on the Adsorption of Water and Methane

Minerals in shales, such as clay minerals, quartz, carbonate minerals and pyrite, have certain impacts on the occurrence and distribution of water, thus affecting the methane adsorption capacity.

Clay minerals are characterized by a very small particle size and a large surface area with a cation exchange ability, and they can easily combine with water to form adsorbed water. Therefore, clay minerals are usually considered to be hydrophilic [31,81,104,115,116,180,181]. However, different types of clay minerals have different structure and surface properties, and their hydrophilicity and influence on gas adsorption are variable [71,88,108,113,182]. Hatch et al. (2012) investigated the water adsorption capacity of montmorillonite, illite and kaolinite (the samples were acquired from the American Clay Mining Society) and found that montmorillonite had a variety of absorbent mechanisms, including external surface adsorption, interlayer water absorption expansion and capillary force adsorption, and had the highest water absorption capacity, while illite and kaolinite (both of which are non-expansive clays) only adsorbed water through their multiple layer structures, with a low

water absorption capacity. Comparatively, the water absorption capacity of illite was slightly higher than that of kaolinite because of the diversity of its micropore and mesopore structures. According to these data, at the same relative humidity (such as 80%), the moisture content of montmorillonite is 2–3 times that of illite and kaolinite (Figure 7) [108]. These results are similar to the equilibrium moisture contents of montmorillonite, illite and kaolinite from the Early Jurassic shales of British Columbia reported by Ross and Bustin (2009), which were 19%, 5.9% and 2.9%, respectively [9].

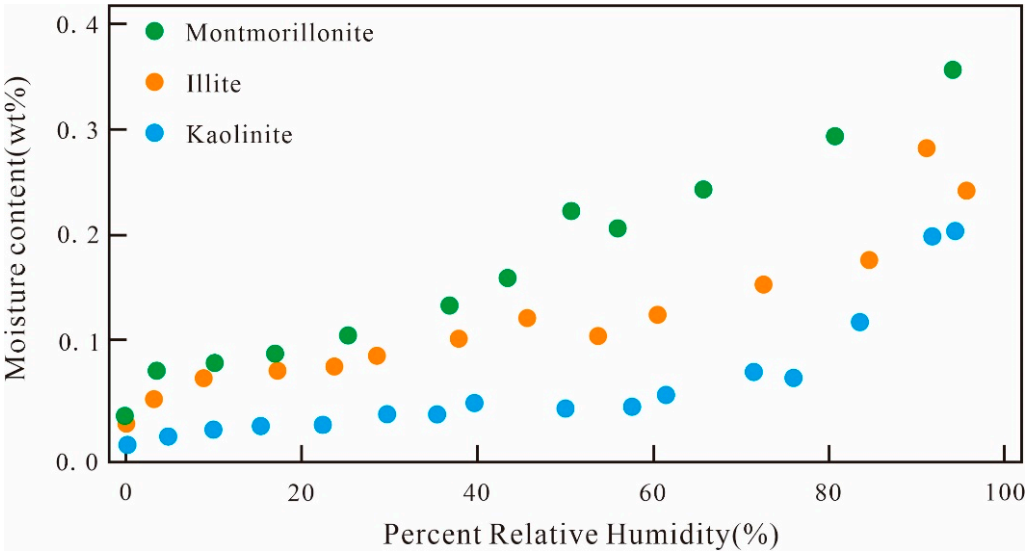

Figure 7. Water adsorption capacities of different types of clay minerals under different humidity conditions (modified from [108]).

Figure 8 shows the relationships between the clay mineral content of shales and their equilibrium adsorption moisture content, connate water content and methane adsorption capacity under equilibrium moisture conditions. There is a clear, positive correlation between the clay mineral content and moisture content (Figure 8a,b), which shows that clay minerals play a major role in controlling the water content in shales owing to their strong hydrophilicity. According to the results reported by Xu et al. (2022) in a study of connate water in Lower Paleozoic over-mature shales from southeast Chongqing, China, the water in inorganic and organic pores averages 68.15% and 31.85%, respectively [40]. The authors found that there is no significant correlation between the clay mineral content and methane adsorption capacity under moist conditions (Figure 8c) and believed that this is because methane adsorption is mainly controlled by the TOC content. Sun et al. (2020) reported correlations between the GIP content (mostly adsorbed gas) of Longmaxi shale samples from the XK2 well in the Xishui Block, Guizhou, China, and the connate water content and mineral composition. Although the clay mineral content showed no clear correlation with the GIP content, it showed a clear, positive correlation with the GIP/TOC (the ratio of GIP content to TOC). This indicates that even under moist conditions, clay minerals still have a certain methane adsorption capacity (Figure 8d) [183]. Moreover, Jagadisan et al. (2020) devised a set of experiments to quantify the water adsorption capacities of isolated kerogen samples of different maturities and two pure clay minerals (illite and kaolinite) using the NMR (nuclear magnetic resonance) method. They found that the water adsorption capacity of the pure clay minerals was much greater than that of over-mature kerogen but less than that of low-mature kerogen (Table 3) [184].

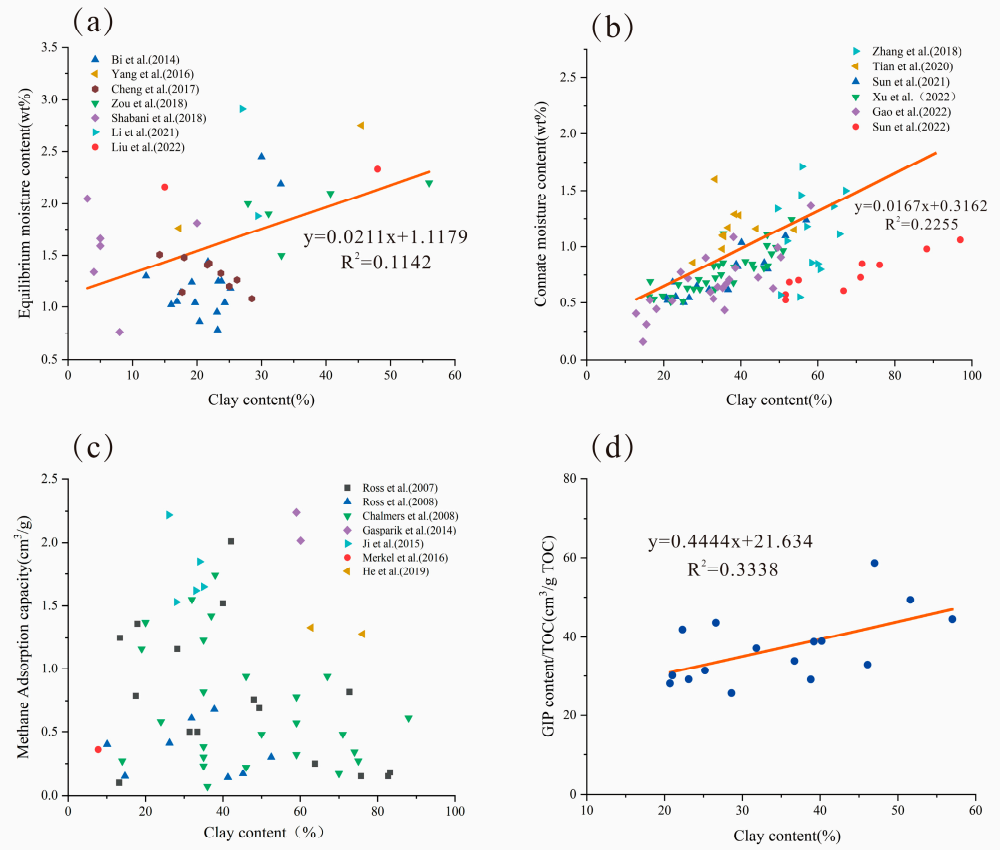

Figure 8. (**a**) Correlation between clay minerals and equilibrium moisture content. The data are from [64,74,89,91,130,185,186]. (**b**) Correlation between clay minerals and connate water content. The data are from [39,40,71,93,133,187]. (**c**) Correlation between clay minerals and methane adsorption capacities of shales containing equilibrium moisture (pressure 6Mpa, temperature 303–318 K). The data sources are as follows: Gordondale and Muskwa shale in British Columbia, Canada [5,85]; Lower Cretaceous shales in northeastern British Columbia, Canada [33]; alum shale in southern Scandinavia [35]; the Longmaxi Formation shale in southeast Chongqing, China [24]; the LOS shale in the Midland Valley Basin, Scotland [87]; the Longmaxi Formation shale from well JSC1, Guizhou, China [188]. (**d**) The correlation between the GIP/TOC and clay mineral content. The data are from the Longmaxi Formation shale from the XK2 well in the Xishui Block, Guizhou, China [183].

Table 3. Water adsorption capacities of isolated kerogen samples and pure clay minerals (data from [184]).

Sample	Water Adsorption Capacity (mL/100 g)
* K1	5.31
* K2	1.90
* K3	0.09
Illite	4.01
Kaolinite	2.15

* K1 is low-mature kerogen (HI is 328 mg-HC/g-OC), K3 is over-mature kerogen (HI is 54 mg-HC/g-OC), and the maturity of K2 is between K1 and K3 (HI is 70 mg-HC/g-OC).

Although it is generally believed that the hydrophilicity of brittle minerals is weak, there are also differences in hydrophilicity between quartz, feldspar, carbonate minerals (dolomite, calcite) and pyrite. Tabrizy et al. (2011) determined the wetting states of quartz, kaolinite and calcite according to the shape of their vapor adsorption isotherms and calculated their number of adsorbed water molecule layers at a relative vapor pressure (P/Po) of 0.15. The results showed that the hydrophilicity order of these minerals is

quartz > kaolinite > calcite, with the numbers of adsorbed water layers being 1.13, 0.52 and 0.19, respectively [189]. Chen et al. (2019c) studied the water occurrence characteristics of the Wufeng-Longmaxi Formation shale from the Changning-Weiyuan block, Sichuan Basin, China, and indicated that the hydrophilicities of quartz and feldspar were similar and stronger than that of calcite [190]. The hydroxyl group on the surface of calcite cannot interact with water molecules, while quartz containing silanol groups can form two kinds of hydrogen bonds with water, which is the basic reason for the weaker hydrophilicity of calcite surfaces compared to quartz [191]. Chai et al. (2019) used the molecular dynamics simulation method to study the adsorption of oil and water on the surfaces of calcite and dolomite and found that their surfaces had a stronger interaction with water molecules than with oil molecules, and the adsorption of water molecules on the surface of dolomite was stronger than that of calcite, with a closer arrangement [192]. Wu et al. (2018) measured the oil and water contact angle of pyrite in shales and found that pyrite often coexisted with organic matter, and it had a strong hydrophobicity [193]. It must be noted that the nanopores of these brittle minerals in shales are generally undeveloped. Moreover, their water content is quite low, and they have little influence on the methane adsorption capacity of shales.

To sum up, there are great differences in hydrophilicity between different minerals, and their effects on the methane adsorption of shales are also different. Their different structures and surface properties are the two basic factors that influence their hydrophilicity. Clay minerals are a kind of main mineral component that affect the adsorption performance of shales, and they can absorb both water and methane. However, the question of how to quantitatively evaluate the methane adsorption capacity of different types of clay minerals under geological conditions (containing connate water) needs to be studied further.

5. Pore Property

According to the pore size classification proposed by the International Union of Pure and Applied Chemistry (IUPAC), nanopores in shales can be further divided into micropores (<2 nm), mesopores (2–50 nm) and macropores (>50 nm). As mentioned above, under geological conditions, adsorbed gas in shales mainly exists in the nanopores of organic matter, and water is mainly stored in the pores of clay minerals, although both water and gas can coexist in the two types of pores. Moreover, the nanopore characteristics of shales (such as their morphology, heterogeneity and pore size distribution) further impact the occurrence and distribution of water and thus affect the adsorbed gas. Based on the results of N_2 adsorption experiments on shale samples from the Longmaxi Formation in Sichuan Basin, China, Li (2018b) quantified the distribution of water in the nanopores and highlighted that the slit pores were more conducive to the occurrence of water than the circular tube pores [194]. Sun et al. (2021a) conducted a comparative study on the fractal dimensions of the Longmaxi Formation shale from northern Guizhou, China, between water-bearing and dry conditions and found that the TOC content showed a significant positive correlation with D1 (the fractal dimension of the pore surface, indicating the heterogeneity of the pores) under both conditions, and the correlation of the moist samples was better than that of the dry samples [195]. This indicates that water in shale tends to accumulate preferentially in the pores, with a stronger heterogeneity in organic nanopores.

In recent years, some progress has been made in research on water distribution in nanopores of different sizes in shales. Here, we discuss some examples. Ruppert et al. (2013) studied the pore distribution characteristics of Barnett shale containing connate water using the small-angle neutron scattering (a measuring range of 100 nm–10 μm) and ultra-small-angle neutron scattering (a measurement range < 250 nm) techniques [196]. Their results show that water molecules preferentially enter pores sized <30 nm (Figure 9a). Cheng et al. (2017) studied the water distribution of over-mature shale containing equilibrium moisture (Lower Cambrian, North Guizhou, China) and observed that the adsorbed water mainly accumulated in mesopores of 3–10 nm, although a small amount of water was also detected in the micropores, macropores and mesopores of other sizes (Figure 9b) [64].

Li et al. (2019) used the NMR technique to evaluate the distribution of self-adsorbed water in marine shales from the southern Sichuan Basin, China, and also found that the adsorbed water was mainly distributed in the mesopores of a size of < 10 nm, while the free water mainly accumulated in pores of a size of > 10 nm, and both types of water were influenced by the pore morphology (Figure 9c) [122]. Hu et al. (2019) studied the water isothermal adsorption of Longmaxi shale samples from the Changning and Weiyuan blocks, Sichuan Basin, China, with different water saturations, and their data showed that water mainly existed in the micropores and mesopores but was rare in the macropores (Figure 9d) [29]. Zou et al. (2020) studied the distribution of equilibrium moisture in Bakken shale samples and their isolated kerogen. The results showed that both the shale and kerogen could adsorb water molecules, and the adsorbed water altered the pore size distribution characteristics, especially in case of the pores with sizes of > 16 nm and between 0.4 nm and 16 nm [37]. Due to differences between shales or research methods, there are some differences in the results reported in the abovementioned studies, but it can be argued that the mesopores in shales represent a main pore size range for water adsorption. It has been shown that pores of a size under a certain critical value will be completely blocked by water due to the capillary coagulation effect, while for pores of a size greater than the critical value, water can exist on their surfaces in the form of a water film [118,190,197]. For example, Hu et al. (2015) investigated the water distribution in kerogen nanopores using the molecular simulation method and proposed that when the pores were smaller than 0.9 nm, the hydrophobic force of the organic matter prevented liquid water from entering these pores, but when the pores were larger than 1.2 nm, the water could enter these pores [118]. This may explain why only a small amount of water exists in micropores. In addition, compared with macropores, mesopores in shales occupy a greater proportion of the specific surface area of non-micropores so that adsorbed water mainly exists in the mesopores rather than the macropores. Therefore, the competition for adsorption between water and methane is related to pore size. Water molecules have a minor influence on micropores, especially organic matter micropores, owing to their small size and/or hydrophobic effect, and as a result, methane absorption occurs predominantly in micropores. The competition for adsorption between water and methane mainly occurs in mesopores, because clay minerals mainly develop mesopores, and mesopores, especially those sized [2–10], are generally dominant in shale nanopore systems (Figure 9b,d).

The methane adsorption capacity of shales is mainly controlled by the specific surface area; thus, these aspects have a clear, positive correlation [198–200]. At a certain temperature and pressure, water molecules compete for the specific surface area to reduce the methane adsorption capacity [201]. Sun et al. (2022) studied the connate water content of carboniferous coal-measure shale from the Yangquan block, Qinghai Basin, China, its occurrence characteristics in nanopores and its influence on methane adsorption performance [39]. According their data, the water in the shale was in an ultra-low saturation state and occurred mainly in clay minerals (91% on average), but its its effective pore structure parameters were significantly decreased, especially the non-micropore-specific surface area (decreased by 70.21% on average), and its methane adsorption capacity was reduced (by 33% on average). Gao et al. (2022a) conducted a comparative study on the pore structure of Longmaxi shale from the Luzhou block, Sichuan Basin, China, under dry and moist (i.e., connate water) conditions. The results indicated that the water significantly decreased the effective pore space of the shale (by approximately 40%) and had greater influences on the structure of the non-micropores and inorganic pores than on the micropores and organic pores, occupying most of the surface area of the non-micropores (76.35% on average), and the micropores were mainly responsible for the shale adsorbed gas [75].

Therefore, the occurrence and distribution of gas and water in shales are directly controlled by their nanopore characteristics, especially the pore structure, and the competition for adsorption between methane and water is related to their adsorption mechanisms (for methane, this is basically physisorption, while for water, it is a combination of chemisorption and physisorption) [98]. However, there are still challenges in determining the occur-

rence and distribution of gas and water in different types and various sizes of nanopores in shales [62,63,122] and in understanding changes in the competitive adsorption mechanisms of shales of different maturities. More in-depth work should be conducted.

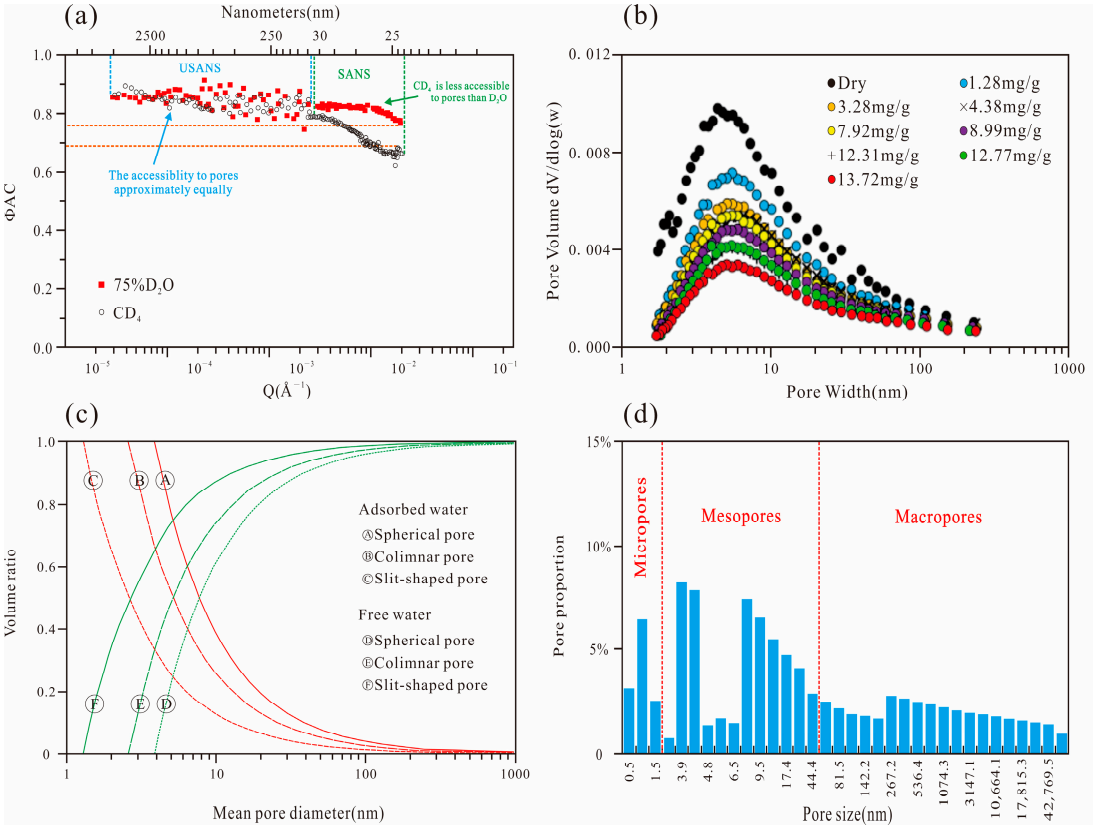

Figure 9. (**a**) Comparison between deuterated water (D_2O) and deuterated methane (CD_4) based on their access to pores in shale samples. ΦAC is the proportion of accessible pores, and Q is the small-angle scattering vector. Barnett shale, Fort Worth Basin, Texas, USA. The figure is modified from [196]. (**b**) Pore size distribution of shale samples with different adsorbed moisture contents. Lower Cambrian shale, Guizhou, China. The figure is from [64]. (**c**) The distribution characteristics of adsorbed water and free water in pores of different shapes in shale. The volume ratio is the ratio of adsorbed water volume or free water volume to the total water volume. Longmaxi shale, Sichuan Basin, China. The figure is from [122]. (**d**) The distribution of adsorbed water in full-sized pores under conditions where the water saturation is below the critical level of water saturation. The ordinate is the ratio of pores of specific sizes which are occupied by water to the total pore volume occupied by water. The mesopores have a stronger water adsorption capacity. Longmaxi shale, Sichuan Basin, China. The figure is from [29].

6. Temperature and Pressure

In addition to the inherent properties of shales themselves, some external environmental factors, such as the pressure and temperature of shale reservoirs, also affect the occurrence and distribution of water, thus changing the methane adsorption capacity [35,89,94]. Li et al. (2020) studied the effects of different pressures on the methane adsorption capacity of Longmaxi shale samples from the Pengshui Block, Guizhou, China, under dry and moist (equilibrium moisture) conditions [202]. The results showed that with increasing pressure, the difference in the methane adsorption capacity of the shales between dry and moist conditions gradually decreased, and the reduction below 2.0 Mpa was twice that below 20.0 Mpa (Figure 10a). Huang et al. (2022) conducted a study similar to that of Li et al. (2020) on Upper Ordovician shale samples from the western part of the Ordos Basin, China. Their results showed that the ratio of methane adsorption capacity under moist conditions

(equilibrium moisture) to that under dry conditions increased from 13.57% at 2.0 Mpa to 20.54% at 30 Mpa (Figure 10b), which also indicates that an increase in pressure can reduce the influence of water on methane adsorption to some extent [203]. This may be because it is difficult for methane to overcome the water resistance of water-bearing pores at a low pressure, but these pores will be reconnected at a high pressure, which changes the distribution of water in shale nanopore systems and weakens the influence of water on the methane adsorption capacity.

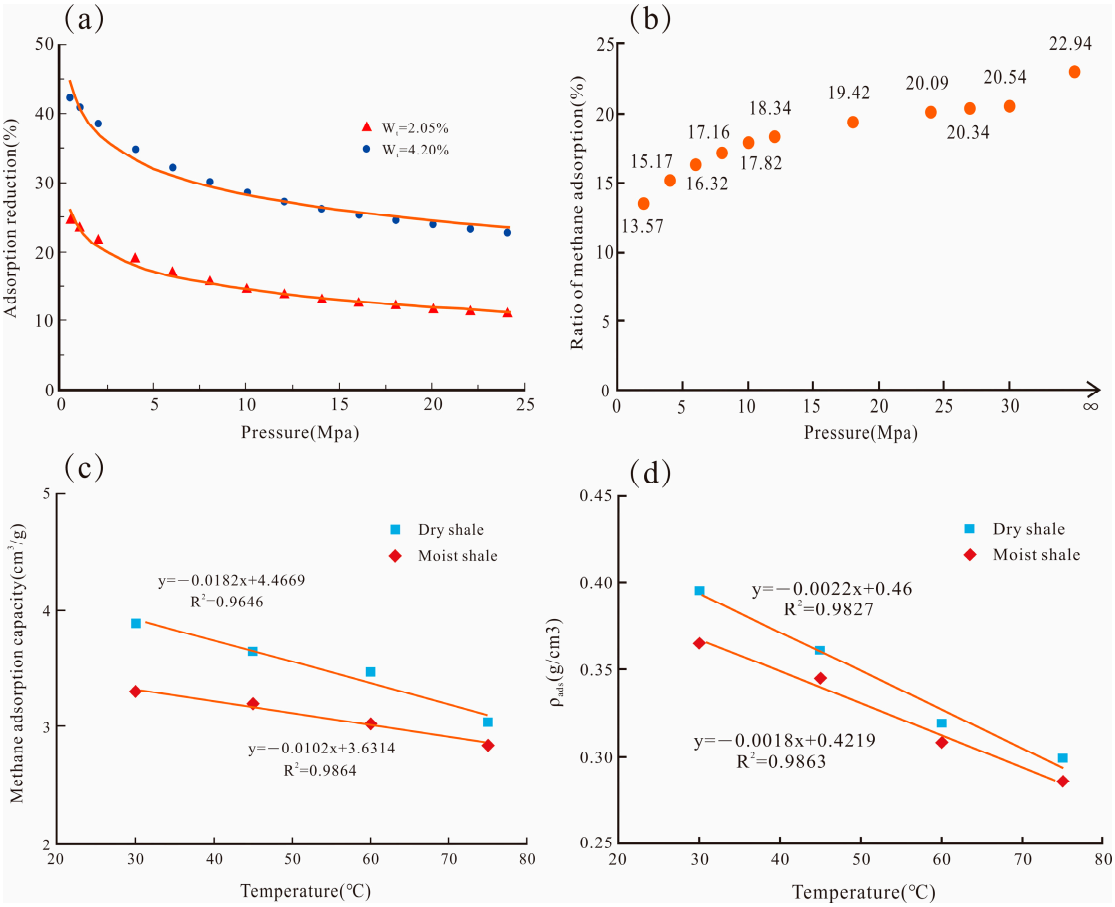

Figure 10. Effects of temperature and pressure on the methane adsorption capacity of shales under dry and moist conditions. (**a**) The relationship between pressure and the reduction percentage of the methane adsorption capacity of moist (equilibrium moisture) shale compared with dry shale. The moisture contents are 2.05% and 4.20%, and the temperature is 333.15 K. The shale samples are from the Longmaxi formation in the Pengshui Block, eastern Sichuan, China. The figure is from [202]. (**b**) The relationship between pressure and the percentage of the methane adsorption capacity of shale containing equilibrium moisture relative to dry samples. The moisture content is 1.15%, and the temperature is 303.15 K. Upper Ordovician shale from the western part of the Ordos Basin, China. The figure is from [203]. (**c**,**d**) The relationship of temperature with the methane adsorption capacity and adsorption phase density (ρads) of shale under dry and moist (connate water) conditions, respectively. Carboniferous coal-measure shale in the Yangquan block, Qinshui Basin, China. The figures are modified from [39].

Similarly, an increase in temperature can also reduce the influence of water on methane adsorption. Zou et al. (2019) studied the methane adsorption capacity of dry shales and their moist (equilibrium moisture) samples (the shale samples were from the Perth Basin, Western Australia) at different temperatures (35–60 °C) [204]. The data showed that there was a negative correlation between the temperature and methane adsorption capacity under both conditions. Han et al. (2021) calculated the difference in methane adsorption

capacity between dry shale and sample with equilibrium moisture (the shale samples were from the southeast part of Sichuan Basin, China), and it decreased gradually with the increase in temperature from 30 °C to 80 °C [96]. Sun et al. (2022) systematically studied the methane adsorption characteristics of coal-measure shale from the Yangquan block, Qinshui Basin, China, under dry and moist (connate water) conditions at different temperatures (30–75 °C) and also found that the temperature restricted the effect of water on the methane adsorption capacity to a certain extent, and the differences in both the methane adsorption capacity and adsorption phase density under dry and wet conditions gradually decreased with the increasing temperature (Figure 10c,d) [39]. The reason for this trend may be that the increase in temperature reduces the methane adsorption capacity of all the adsorption sites, while water only affects the adsorption sites in inorganic pores and some organic pores, such as those with oxygen-containing functional groups, and the increase in temperature also releases some adsorption sites occupied by water, which weakens the influence of the water [31,90,178,205].

Although both pressure and temperature have certain influences on the methane adsorption of water-bearing shales, the effects are variable for shale gas reservoirs with different burial depths. The proportion of adsorbed gas (the ratio of adsorbed gas to total gas) in shale reservoirs is relatively high in a depth range of 500–2000 m, in which it is greatly influenced by water. With the increase in the burial depth, the proportion of adsorbed gas clearly decreases, and the influence of water also decreases. Deep and ultra-deep shale gas is an important target for future exploration and development [206–208], but the occurrence and distribution of water in high-temperature and -pressure environments and its effect on adsorbed gas remain to be explored further.

7. Conclusions

In this paper, the main controlling factors and mechanisms of water adsorption in shales and water's effects on the methane adsorption capacity of shales or adsorbed gas were reviewed. The adsorption capacity of shales for water and methane is not only controlled mainly by their geochemical attributes, such as the organic matter properties (including the TOC content, kerogen type and maturity), inorganic mineral composition and pore characteristics, but also restricted by some external factors, such as pressure and temperature, to a certain extent. A certain amount of water can be adsorbed in the organic nanopores of shales, and with the increase in the TOC content, the influence of water on the adsorption capacity of shales can be restricted to a certain extent. Under water-bearing conditions, the TOC content of shales is still the main factor controlling their methane adsorption capacity. In the low- and middle-mature stages, different types of kerogen or macerals in shales have different chemical structures, especially oxygen-containing functional groups, which lead to different hydrophilicities and methane adsorption capacities. With increasing maturity, the functional groups of organic matter in shales are gradually eliminated, the chemical structures tend to become similar, and a large number of organic nanopores form in the high- and over-mature stages, resulting in a high capillary force, which enables the organic matter to still absorb a small amount of water. Different mineral components in shales have different adsorption capacities for water, especially in regard to the hydrophilicity of different types of clay minerals. The strong hydrophilicity of clay minerals is the main mechanism of water adsorption in shales, but even under saturated adsorption water conditions, clay minerals still have a certain methane adsorption capacity. The pore morphology, heterogeneity and pore size distribution of shales all have certain effects on the water adsorption capacity. Compared with micropores and macropores, adsorbed water tends to exist in mesopores, especially the mesopores of clay minerals. Water competes with methane for specific adsorption sites, which leads to a decrease in the methane adsorption capacity of shales with water. In addition, with the increase in pressure and temperature, the influence of water on methane adsorption is weakened to some extent.

The occurrence and distribution of water and methane in the nanopores of shale reservoirs are the comprehensive results of various geological and geochemical factors, and the related mechanism is complex. Therefore, a series of theoretical and practical problems still need to be explored, including the following: the change in the hydrophilicity of organic matter and clay minerals and its relationship with the evolution of their nanopore characteristics during the thermal evolution of shales, especially the difference in methane adsorption capacity between shales with different types of kerogen under water-bearing conditions; the methane adsorption capacities of different types of clay minerals under water-bearing conditions and their contribution to shale gas; and the competitive adsorption behavior of water and methane in shale nanopores and its thermodynamic mechanism, especially the evaluation and prediction of shale adsorption gas in the presence of non-hydrocarbon gases (such as N_2 and CO_2). In addition, challenges also exist in determining the occurrence and distribution of gas and water in different types of nanopores and nanopores of different sizes in shales, and we still lack an effective means and theoretical models to test and predict the effect of water on methane adsorption under high-temperature and high-pressure conditions. These issues are important directions for future research on shale gas reservoir evaluation.

Author Contributions: Conceptualization, Y.X., X.X. and Q.Z.; methodology, Y.X.; software, Y.X.; validation, W.L. and Y.Z.; formal analysis, Y.X.; investigation, Y.X.; resources, X.X. and Q.Z.; data curation, Y.X.; writing—original draft preparation, Y.X.; writing—review and editing, X.X.; visualization, Y.X.; supervision, X.X.; project administration, X.X.; funding acquisition, X.X. All authors have read and agreed to the published version of the manuscript.

Funding: This research was funded by the Science and Technology Department of Shanxi Province, China (20201101003), and the National Natural Science Foundation of China (42030804; 42272140; 41502161).

Data Availability Statement: Not applicable.

Acknowledgments: All the editors and anonymous reviewers are gratefully acknowledged.

Conflicts of Interest: The authors declare no conflict of interest.

References

1. Weijermars, R.; Drijkoningen, G.; Heimovaara, T.; Rudolph, E.; Weltje, G.; Wolf, K. Unconventional gas research initiative for clean energy transition in Europe. *J. Nat. Gas Sci. Eng.* **2011**, *3*, 402–412. [CrossRef]
2. Wood, D. Establishing credible reaction-kinetics distributions to fit and explain multi-heating rate S2 pyrolysis peaks of kerogens and shales. *Adv. Geo-Energy Res.* **2018**, *3*, 1–28. [CrossRef]
3. Dai, J.; Qin, S.; Hu, G.; Ni, Y.; Gan, L.; Huang, S.; Hong, F. Major progress in the natural gas exploration and development in the past seven decades in China. *Pet. Explor. Dev.* **2019**, *46*, 1100–1110. [CrossRef]
4. Zou, C.; Pan, S.; Jin, Z.; Gao, J.; Yang, Z.; Wu, S.; Zhao, Q. Shale oil and gas revolution and its impact. *Acta Pet. Sin.* **2020**, *41*, 1–12. (In Chinese with English abstract) [CrossRef]
5. Ross, D.; Bustin, R. Shale gas potential of the Lower Jurassic Gordondale Member, northeastern British Columbia, Canada. *Bull. Can. Pet. Geol.* **2007**, *55*, 51–75. [CrossRef]
6. Zhang, T.; Ellis, G.; Ruppel, S.; Milliken, K.; Yang, R. Effect of organic-matter type and thermal maturity on methane adsorption in shale-gas systems. *Org. Geochem.* **2012**, *47*, 120–131. [CrossRef]
7. Ambrose, R.; Hartman, R.; Diaz-Campos, M.; Yucel Akkutlu, I.; Sondergeld, C. Shale Gas-in-Place Calculations Part I: New Pore-Scale Considerations. *SPE J.* **2012**, *17*, 219–229. [CrossRef]
8. Hao, F.; Zou, H.; Lu, Y. Mechanisms of shale gas storage: Implications for shale gas exploration in China. *AAPG Bull.* **2013**, *97*, 1325–1346. [CrossRef]
9. Ross, D.; Marc, B. The importance of shale composition and pore structure upon gas storage potential of shale gas reservoirs. *Mar. Pet. Geol.* **2009**, *26*, 916–927. [CrossRef]
10. Nelson, P. Pore-throat sizes in sandstones, tight sandstones, and shales. *AAPG Bull.* **2009**, *93*, 329–340. [CrossRef]
11. Ji, L.; Zhang, T.; Milliken, K.; Qu, J.; Zhang, X. Experimental investigation of main controls to methane adsorption in clay-rich rocks. *Appl. Geochem.* **2012**, *27*, 2533–2545. [CrossRef]
12. Zou, C.; Zhao, Q.; Dong, D.; Yang, Z.; Qiu, Z.; Liang, F.; Wang, N.; Huang, Y.; Duan, A.; Zhang, Q.; et al. Geological characteristics, main challenges and future prospect of shale gas. *Nat. Gas Geosci.* **2017**, *28*, 1781–1796. [CrossRef]
13. Li, J.; Chen, Z.; Wu, K.; Wang, K.; Luo, J.; Feng, D.; Qu, S.; Li, X. A multi-site model to determine supercritical methane adsorption in energetically heterogeneous shales. *Chem. Eng. J.* **2018**, *349*, 438–455. [CrossRef]

14. Curtis, J.B. Fractured shale-gas systems. *AAPG Bull.* **2002**, *86*, 1921–1938.
15. Jarvie, D.M. *Shale Resource Systems for Oil and Gas: Part2-Shale-Oil Resource Systems. Shale Reservoirs-Giant Resources for the 21st Century*; Worldwide Geochemistry, LLC.: Humble, TX, USA, 2012.
16. Chen, L.; Zuo, L.; Jiang, Z.; Jiang, S.; Liu, K.; Tang, J.; Zhang, L. Mechanisms of shale gas adsorption: Evidence from thermodynamics and kinetics study of methane adsorption on shale. *Chem. Eng. J.* **2019**, *361*, 559–570. [CrossRef]
17. Wu, S.; Guo, J.; Li, Z.; Qin, M.; Huang, Y.; He, H. Identification and optimization of shale gas "sweet spots" in marine Niutitang Formation, South China. *Oil Gas Geol.* **2020**, *41*, 1048–1059.
18. Gou, Q.; Xu, S.; Hao, F.; Zhang, B.; Shu, Z.; Yang, F.; Wang, Y.; Li, Q. Quantitative calculated shale gas contents with different lithofacies: A case study of Fuling gas shale, Sichuan Basin, China. *J. Nat. Gas Sci. Eng.* **2020**, *76*, 103222. [CrossRef]
19. Qiao, J.; Littke, R.; Zieger, L.; Jiang, Z.; Fink, R. Controls on gas storage characteristics of Upper Paleozoic shales from the southeastern Ordos Basin. *Mar. Pet. Geol.* **2020**, *117*, 104377. [CrossRef]
20. Shi, X.; Zhou, S.; Tian, C.; Li, D.; Li, D.; Li, Y.; Wu, W.; Cai, C.; Chen, Y. Methane adsorption characteristics and controlling factors of deep shale gas in southern Sichuan Basin, China. *J. Nat. Gas Geosci.* **2021**, *32*, 1735–1748.
21. Lu, C.; Chen, L.; Jing, C.; Tan, X.; Nie, Z.; Chen, X.; Heng, D. Gas-Bearing Characteristics of the Longmaxi Formation Shale in the Changning Area, Southern Sichuan Basin, SW China. *Front. Earth Sci.* **2022**, *10*, 755690. [CrossRef]
22. Gasparik, M.; Ghanizadeh, A.; Bertier, P.; Gensterblum, Y.; Bouw, S.; Krooss, B.M. High-Pressure Methane Sorption Isotherms of Black Shales from The Netherlands. *Energy Fuels* **2012**, *26*, 4995–5004. [CrossRef]
23. Rexer, T.F.; Mathia, E.J.; Aplin, A.C.; Thomas, K.M. High-pressure methane adsorption and characterization of pores in Posidonia shales and isolated kerogens. *Energy Fuels* **2014**, *28*, 2886–2901. [CrossRef]
24. Ji, W.; Song, Y.; Jiang, Z.; Chen, L.; Li, Z.; Yang, X.; Meng, M. Estimation of marine shale methane adsorption capacity based on experimental investigations of Lower Silurian Longmaxi formation in the Upper Yangtze Platform, south China. *Mar. Pet. Geol.* **2015**, *68*, 94–106. [CrossRef]
25. Jarvie, D.M.; Liu, B.; Schieber, J.; Mastalerz, M.; Cichon-Pupienis, A.; Littke, R.; Froidl, F.; Kong, X.; Jiang, Z.; Han, C. Shale resource systems for oil and gas: Part 1—Shale-gas resource systems. *AAPG Mem.* **2012**, *97*, 69–87.
26. Ahmad, M.; Haghighi, M. Water Saturation Evaluation of Murteree and Roseneath Shale Gas Reservoirs, Cooper Basin, Australia Using Wire-line Logs, Focused Ion Beam Milling and Scanning Electron Microscopy. In Proceedings of the SPE Unconventional Resources Conference and Exhibition-Asia Pacific, Brisbane, Australia, 11–13 November 2013.
27. Fang, C.; Huang, Z.; Wang, Q.; Zheng, D.; Liu, H.-L. Cause and significance of the ultra-low water saturation in gas-enriched shale reservoir. *Nat. Gas Geosci.* **2014**, *25*, 471–476.
28. Merkel, A.; Fink, R.; Littke, R. The role of pre-adsorbed water on methane sorption capacity of Bossier and Haynesville shales. *Int. J. Coal Geol.* **2015**, *147*, 1–8. [CrossRef]
29. Hu, Z.; Duan, X.; He, Y. Influence of reservoir primary water on shale gas occurrence and flow capacity. *Nat. Gas Ind. B* **2019**, *6*, 71–78. [CrossRef]
30. Jin, Z.; Firoozabadi, A. Effect of water on methane and carbon dioxide sorption in clay minerals by Monte Carlo simulations. *Fluid Phase Equilibria* **2014**, *382*, 10–20. [CrossRef]
31. Li, J.; Li, X.; Wang, X.; Li, Y.; Wu, K.; Shi, J.; Yang, L.; Feng, D.; Zhang, T.; Yu, P. Water distribution characteristic and effect on methane adsorption capacity in shale clay. *Int. J. Coal Geol.* **2016**, *159*, 135–154. [CrossRef]
32. Whitelaw, P.; Uguna, C.; Stevens, L.; Meredith, W.; Snape, C.; Vane, C.; Moss-Hayes, V.; Carr, A. Shale gas reserve evaluation by laboratory pyrolysis and gas holding capacity consistent with field data. *Nat. Commun.* **2019**, *10*, 3659. [CrossRef]
33. Chalmers, G.; Bustin, R. Lower Cretaceous gas shales in northeastern British Columbia, Part I: Geological controls on methane sorption capacity. *Bull. Can. Pet. Geol.* **2008**, *56*, 1–21. [CrossRef]
34. Gensterblum, Y.; Merkel, A.; Busch, A. High-pressure CH_4 and CO_2 sorption isotherms as a function of coal maturity and the influence of moisture. *Int. J. Coal Geol.* **2013**, *118*, 45–57. [CrossRef]
35. Gasparik, M.; Bertier, P.; Gensterblum, Y.; Ghanizadeh, A.; Krooss, B.; Littke, R. Geological controls on the methane storage capacity in organic-rich shales. *Int. J. Coal Geol.* **2014**, *123*, 34–51. [CrossRef]
36. Chen, S.; Han, Y.; Fu, C.; Zhang, H.; Zhu, Y.; Zuo, Z. Micro and nano-size pores of clay minerals in shale reservoirs: Implication for the accumulation of shale gas. *Sediment Geol.* **2016**, *342*, 180–190. [CrossRef]
37. Zou, J.; Rezaee, R.; Yuan, Y.; Liu, K.; Xie, Q.; You, L. Distribution of adsorbed water in shale: An experimental study on isolated kerogen and bulk shale samples. *J. Pet. Sci. Eng.* **2020**, *187*, 106858. [CrossRef]
38. Wang, M.; Lun, Z.; Zhao, C.; Wang, H.; Luo, C.; Fu, X.; Li, C.; Zhang, D. Influences of Primary Moisture on Methane Adsorption within Lower Silurian Longmaxi Shales in the Sichuan Basin, China. *Energy Fuels* **2020**, *34*, 10810–10824. [CrossRef]
39. Sun, J.; Xiao, X.; Cheng, P. Methane absorption of coal-measure shales with and without pore water from the Qinshui Basin, North China: Based on high-pressure methane absorption experiments. *Int. J. Coal Geol.* **2022**, *263*, 104116. [CrossRef]
40. Xu, L.; Wei, H.; Chen, L.; Liu, L.; Jiang, Z.; Yang, K.; Li, X. Storing characteristics and main controlling factors of connate water in lower Paleozoic shales in southeast Chongqing, China. *J. Pet. Sci. Eng.* **2022**, *215*, 110543. [CrossRef]
41. Bennion, D.; Bietz, R.; Thomas, F. Reductions in the productivity of oil and low permeability gas-reservoirs due to aqueous-phase trapping. *J. Can. Pet. Technol.* **1994**, *33*, 45–54. [CrossRef]
42. Wang, F.; Reed, R.; John, A.; Katherine, G. Pore Networks and Fluid Flow in Gas Shales. In Proceedings of the SPE Annual Technical Conference and Exhibition, New Orleans, LA, USA, 4–7 October 2009.

43. Day-Stirrat, R.; Milliken, K.; Dutton, S.; Loucks, R.; Hillier, S.; Aplin, A.; Schleicher, A. Open-system chemical behavior in deep Wilcox Group mudstones, Texas Gulf Coast, USA. *Mar. Pet. Geol.* **2010**, *27*, 1804–1818. [CrossRef]
44. Dehghanpour, H.; Lan, Q.; Saeed, Y.; Fei, H.; Qi, Z. Spontaneous Imbibition of Brine and Oil in Gas Shales: Effect of Water Adsorption and Resulting Microfractures. *Energy Fuels* **2013**, *27*, 3039–3049. [CrossRef]
45. Makhanov, K.; Habibi, A.; Dehghanpour, H.; Kuru, E. *Liquid Uptake of Gas Shales: A Workflow to Estimate Water Loss during Shut-in Periods after Fracturing Operations*; Department of Geophysics, Stanford University: Stanford, CA, USA, 2014; Volume 7, pp. 22–32.
46. Vidic, R.D.; Brantley, S.; Vandenbossche, J.; Yoxtheimer, D.; Abad, J. Impact of Shale Gas Development on Regional Water Quality. *Science* **2013**, *340*, 1235009. [CrossRef] [PubMed]
47. Vengosh, A.; Jackson, R.; Warner, N.; Darrah, T.; Kondash, A. A Critical Review of the Risks to Water Resources from Unconventional Shale Gas Development and Hydraulic Fracturing in the United States. *Environ. Sci. Technol.* **2014**, *48*, 8334–8348. [CrossRef]
48. Testamanti, M.N.; Rezaee, R. Determination of NMR T2 cut-off for clay bound water in shales: A case study of Carynginia Formation, Perth Basin, Western Australia. *J. Pet. Sci. Eng.* **2017**, *149*, 497–503. [CrossRef]
49. Joubert, J.; Grein, C.; Bienstock, D. Effect of moisture on the methane capacity of American coals. *Fuel* **1974**, *53*, 186–191. [CrossRef]
50. Ambrose, R.; Hartman, R.; Diaz-Campos, M.; Akkutlu, I.; Sondergeld, C. New Pore-scale Considerations for Shale Gas in Place Calculations. In Proceedings of the SPE Unconventional Gas Conference, Pittsburgh, PA, USA, 23–25 February 2010.
51. Xiao, X.; Wang, M.; Wei, Q.; Tian, H.; Pan, L.; Li, T. Evaluation of Lower Paleozoic shale with shale gas prospect in south China. *Nat. Gas Geosci.* **2015**, *26*, 1433–1445.
52. Bennion, D.; Thomas, F. Formation damage issues impacting the productivity of low permeability, low initial water saturation gas producing formations. *J. Energy Resour. Technol.* **2006**, *127*, 240–247. [CrossRef]
53. Bowker, K.A. Barnett Shale gas production, Fort Worth Basin: Issues and discussion. *AAPG Bull.* **2007**, *91*, 523–533. [CrossRef]
54. Boyer, C.; Kieschnick, J.; Suarez-Rivera, R.; Lewis, R.; Waters, G. Producing gas from its source. *Oilfield Rev.* **2008**, *18*, 36–49.
55. Newsham, K.E.; Rushing, J.A.; Lasswell, P.M. Use of Vapor Desorption Data to Characterize High Capillary Pressures in a Basin-Centered Gas Accumulation with Ultra-Low Connate Water Saturations. In Proceedings of the SPE Annual Technical Conference and Exhibition, Denver, CO, USA, 5–8 October 2003.
56. Liu, H.; Wang, H. Characteristics of ultra-low water saturation of marine shale in southern China and selection index of overpressure core area. *Nat. Gas Ind.* **2013**, *33*, 140–144. (In Chinese with English abstract)
57. Cheng, P.; Xiao, X.; Tian, H.; Wang, X. Water Content and Equilibrium Saturation and Their Influencing Factors of the Lower Paleozoic Overmature Organic-Rich Shales in the Upper Yangtze Region of Southern China. *Energy Fuels* **2018**, *32*, 11452–11466. [CrossRef]
58. Yee, D.; Seidle, J.; Hanson, W.; Law, B.; Rice, D. Gas Sorption on Coal and Measurement of Gas Content. In *Hydrocarbons from Coal*; American Association of Petroleum Geologists: Tulsa, OK, USA, 1993; Volume 38.
59. Krooss, B.; Bergen, F.; Gensterblum, Y.; Siemons, N.; Pagnier, H.; David, P. High-pressure methane and carbon dioxide adsorption on dry and moisture-equilibrated Pennsylvanian coals. *Int. J. Coal Geol.* **2002**, *51*, 69–92. [CrossRef]
60. Kadoura, A.; Narayanan Nair, A.; Sun, S. Adsorption of carbon dioxide, methane, and their mixture by montmorillonite in the presence of water. *Microporous Mesoporous Mater.* **2016**, *225*, 331–341. [CrossRef]
61. Fan, K.; Li, Y.; Elsworth, D.; Dong, M.; Yin, C.; Li, Y.; Chen, Z. Three stages of methane adsorption capacity affected by moisture content. *Fuel* **2018**, *231*, 352–360. [CrossRef]
62. Hartman, R.; Lasswell, P.; Bhatta, N. Recent Advances in the Analytical Methods Used for Shale Gas Reservoir Gas-in-Place Assessment. *Search Discov.* **2008**, *40317*, 20–23.
63. Handwerger, D.; Suarez-Rivera, R.; Vaughn, K.; Keller, J. Improved Petrophysical Core Measurements on Tight Shale Reservoirs Using Retort and Crushed Samples. In Proceedings of the SPE Annual Technical Conference and Exhibition, Denver, CO, USA, 30 October–2 November 2011.
64. Cheng, P.; Tian, H.; Xiao, X.; Gai, H.; Li, T.; Wangt, X. Water Distribution in Overmature Organic-Rich Shales: Implications from Water Adsorption Experiments. *Energy Fuels* **2017**, *31*, 13120–13132. [CrossRef]
65. Cheng, P.; Xiao, X.; Tian, H.; Gai, H.; Zhou, Q.; Li, T.; Fan, Q. Differences in the distribution and occurrence phases of pore water in various nanopores of marine-terrestrial transitional shales in the Yangquan area of the northeast Qinshui Basin, China. *Mar. Pet. Geol.* **2022**, *137*, 105510. [CrossRef]
66. Yuan, Y.; Rezaee, R.; Verrall, M. Pore characterization and clay bound water assessment in shale with a combination of NMR and low-pressure nitrogen gas adsorption. *Int. J. Coal Geol.* **2018**, *194*, 11–21. [CrossRef]
67. Hu, M.; Wang, J. Laboratory measurement of water imbibition into low-permeability welded tuff. *J. Hydrol.* **2001**, *242*, 64–78. [CrossRef]
68. *ASTM D1412-07*; ASTM Standard Test Method for Equilibrium Moisture of Coal at 96 to 97 Percent Relative Humidity and 30 °C. American Society for Testing and Materials: West Conshohocken, PA, USA, 2007; p. 5.
69. Gasparik, M.; Ghanizadeh, A.; Gensterblum, Y.; Krooss, B. 'Multi-temperature' method for high-pressure sorption measurements on moist shales. *Rev. Sci. Instrum.* **2013**, *84*, 85116. [CrossRef]
70. Wang, L.; Wan, J.; Tokunaga, T. Experimental and modeling study of methane adsorption onto partially saturated shales. *Water Resour. Res.* **2018**, *54*, 5017–5029. [CrossRef]

71. Tian, H.; Wang, M.; Liu, S. Influence of Pore Water on the Gas Storage of Organic-Rich Shale. *Energy Fuels* **2020**, *34*, 5293–5306. [CrossRef]
72. Feng, D.; Li, X.; Wang, X.; Li, J.; Sun, F.; Sun, Z.; Zhang, T.; Li, P.; Chen, Y.; Zhang, X. Water adsorption and its impact on the pore structure characteristics of shale clay. *Appl. Clay Sci.* **2018**, *155*, 126–138. [CrossRef]
73. Li, P.; Zhang, J.; Rezaee, R.; Dang, W.; Tang, X.; Nie, H.; Chen, S. Effect of adsorbed moisture on the pore size distribution of marine-continental transitional shales: Insights from lithofacies differences and clay swelling. *Appl. Clay Sci.* **2021**, *201*, 105926. [CrossRef]
74. Liu, Y.; Cao, Q.; Ye, X.; Dong, L. Adsorption Characteristics and Pore Structure of Organic-Rich Shale with Different Moisture Contents. *Front. Earth Sci.* **2022**, *10*, 863691. [CrossRef]
75. Gao, H.; Cheng, P.; Wu, W.; Liu, S.; Luo, C.; Li, T.; Zhong, K.; Tian, H. Pore Water and Its Influences on the Nanopore Structures of Deep Longmaxi Shales in the Luzhou Block of the Southern Sichuan Basin, China. *Energies* **2022**, *15*, 4053. [CrossRef]
76. Labus, M.A.; Labus, K.a.; Bujok, P.B. Determination of the pore space parameters in microporous rocks by means of thermal methods. *J. Pet. Sci. Eng.* **2015**, *127*, 482–489. [CrossRef]
77. Shen, B.; Li, Z.; Zheng, Z.; Li, C.; Lei, H.; Zhang, L.; Zhu, H.; Lu, S.; Du, M. Status and relative content of water in shale determined by thermogravimetry-mass spectrometry analysis. *J. Pet. Sci. Eng.* **2021**, *196*, 107739. [CrossRef]
78. Dfaz, A.; Roegiers, J. Water distribution: A key factor to characterize shale. In Proceedings of the DC Rocks 2001, The 38th U.S. Symposium on Rock Mechanics (USRMS), Washington, DC, USA, 7–10 July 2001.
79. Mu, Y.; Hu, Z.; Chang, J.; Duan, X.; Li, Y.; Li, Y.; Niu, W. Effect of water occurrence on shale seepage ability. *J. Pet. Sci. Eng.* **2021**, *204*, 108725. [CrossRef]
80. Li, X.; Chen, S.; Wang, Y.; Zhang, Y.; Wang, Y.; Wu, J.; Zhang, J.; Khan, J. Influence of Pore Structure Particularity and Pore Water on the Occurrence of Deep Shale Gas: Wufeng–Longmaxi Formation, Luzhou Block, Sichuan Basin. *Nat. Resour. Res.* **2022**, *31*, 1403–1423. [CrossRef]
81. Zolfaghari, A.; Dehghanpour, H.; Xu, M. Water sorption behaviour of gas shales: II. Pore size distribution. *Int. J. Coal Geol.* **2017**, *179*, 187–195. [CrossRef]
82. Shen, W.; Li, X.; Lu, X.; Wan, Y.; Guo, W.; Zuo, L. Study on Moisture Transport Characteristics of Shale Based on Isothermal Adsorption. *Lixue Xuebao* **2019**, *51*, 932–939.
83. Ren, W.; Guo, J.; Zeng, F.; Wang, T. Modeling of High-Pressure Methane Adsorption on Wet Shales. *Energy Fuels* **2019**, *33*, 7043–7051. [CrossRef]
84. Chalmers, G.; Bustin, R. The organic matter distribution and methane capacity of the Lower Cretaceous strata of Northeastern British Columbia, Canada. *Int. J. Coal Geol.* **2007**, *70*, 223–239. [CrossRef]
85. Ross, D.; Bustin, R. Characterizing the shale gas resource potential of Devonian-Mississippian strata in the Western Canada sedimentary basin: Application of an integrated formation evaluation. *AAPG Bull.* **2008**, *43*, 87–125. [CrossRef]
86. Yuan, W.; Pan, Z.; Li, X.; Yang, Y.; Zhao, C.; Connell, L.; Li, S.; He, J. Experimental study and modelling of methane adsorption and diffusion in shale. *Fuel* **2014**, *117*, 509–519. [CrossRef]
87. Merkel, A.; Fink, R.; Littke, R. High pressure methane sorption characteristics of lacustrine shales from the Midland Valley Basin, Scotland. *Fuel* **2016**, *182*, 361–372. [CrossRef]
88. Wang, L.; Yu, Q. The effect of moisture on the methane adsorption capacity of shales: A study case in the eastern Qaidam Basin in China. *J. Hydrol.* **2016**, *542*, 487–505. [CrossRef]
89. Zou, J.; Rezaee, R.; Xie, Q.; You, L.; Liu, K.; Saeedi, A. Investigation of moisture effect on methane adsorption capacity of shale samples. *Fuel* **2018**, *232*, 323–332. [CrossRef]
90. Crosdale, P.; Moore, T.; Mares, T. Influence of moisture content and temperature on methane adsorption isotherm analysis for coals from a low-rank, biogenically-sourced gas reservoir. *Int. J. Coal Geol.* **2008**, *76*, 166–174. [CrossRef]
91. Yang, F.; Xie, C.; Ning, Z.; Krooss, B. High-Pressure Methane Sorption on Dry and Moisture-Equilibrated Shales. *Energy Fuels* **2016**, *31*, 482–492. [CrossRef]
92. Day, S.; Sakurovs, R.; Weir, S. Supercritical gas sorption on moist coals. *Int. J. Coal Geol.* **2008**, *74*, 203–214. [CrossRef]
93. Sun, J.; Xiao, X.; Wei, Q.; Cheng, P.; Tian, H. Occurrence of Irreducible Water and Its Influences on Gas-Bearing Property of Gas Shales from Shallow Longmaxi Formation in the Xishui Area, Guizhou, Southern China. *Front. Earth Sci.* **2021**, *9*, 654136. [CrossRef]
94. Zhao, T.; Li, X.; Zhao, H.; Li, M. Molecular simulation of adsorption and thermodynamic properties on type II kerogen: Influence of maturity and moisture content. *Fuel* **2017**, *190*, 198–207. [CrossRef]
95. Chen, Z.; Ning, Z.; Wang, Q.; Huang, L.; Qi, R.; Wang, J. Experimental study on methane adsorption characteristics of water-bearing shale. *Fault-Block Oil Gas Field* **2018**, *25*, 510–514+548. (In Chinese with English abstract)
96. Han, W.; Li, A.; Memon, A.; Ma, M. Synergetic Effect of Water, Temperature, and Pressure on Methane Adsorption in Shale Gas Reservoirs. *ACS Omega* **2021**, *6*, 2215–2229. [CrossRef]
97. Xiang, J.; Zeng, F.; Liang, H.; Li, B.; Song, X. Molecular simulation of the $CH_4/CO_2/H_2O$ adsorption onto the molecular structure of coal. *Sci. China Earth Sci.* **2014**, *57*, 1749–1759. [CrossRef]
98. Habibi, A.; Dehghanpour, H. Wetting Behavior of Tight Rocks: From Core Scale to Pore Scale. *Water Resour. Res.* **2018**, *54*, 9162–9186. [CrossRef]

99. Schettler, P.; Parmely, C. Contributions to Total Storage Capacity in Devonian Shales. In Proceedings of the SPE Eastern Regional Meeting, Lexington, KY, USA, 22–25 October 1991.
100. Lu, X.; Li, F.; Watson, A. Adsorption measurements in Devonian shales. *Fuel* **1995**, *74*, 599–603. [CrossRef]
101. Wang, S.; Song, Z.; Cao, T.; Song, X. The methane sorption capacity of Paleozoic shales from the Sichuan Basin, China. *Mar. Pet. Geol.* **2013**, *44*, 112–119. [CrossRef]
102. Yang, F.; Ning, Z.; Zhang, R.; Zhao, H.; Krooss, B. Investigations on the methane sorption capacity of marine shales from Sichuan Basin, China. *Int. J. Coal Geol.* **2015**, *146*, 104–117. [CrossRef]
103. Li, T. *Effect of Water Content on Methane Adsorption in Shale*; China University of Geosciences: Beijing, China, 2019. (In Chinese with English abstract)
104. Sang, G.; Liu, S.; Elsworth, D. Water Vapor Sorption Properties of Illinois Shales Under Dynamic Water Vapor Conditions: Experimentation and Modeling. *Water Resour. Res.* **2019**, *55*, 7212–7228. [CrossRef]
105. Yang, R.; Jia, A.; He, S.; Hu, Q.; Dong, T.; Hou, Y.; Yan, J. Water adsorption characteristics of organic-rich Wufeng and Longmaxi Shales, Sichuan Basin (China). *J. Pet. Sci. Eng.* **2020**, *193*, 107387. [CrossRef]
106. Huang, L.; Ning, Z.; Wang, Q.; Zhang, W.; Cheng, Z.; Wu, X.; Qin, H. Effect of organic type and moisture on CO_2/CH_4 competitive adsorption in kerogen with implications for CO_2 sequestration and enhanced CH_4 recovery. *Appl. Energy* **2018**, *210*, 28–43. [CrossRef]
107. Branson, K.; Newman, A. Water sorption on Ca-saturated clays; I, Multilayer sorption and microporosity in some illites. *Clay Miner.* **1983**, *18*, 277–287. [CrossRef]
108. Hatch, C.; Wiese, J.; Crane, C.; Harris, K.; Kloss, H.; Baltrusaitis, J. Water adsorption on clay minerals as a function of relative humidity: Application of BET and Freundlich adsorption models. *Langmuir ACS J. Surf. Colloids* **2012**, *28*, 1790–1803. [CrossRef]
109. Passey, Q.; Bohacs, K.; Esch, W.; Klimentidis, R.; Sinha, S. From Oil-Prone Source Rock to Gas-Producing Shale Reservoir—Geologic and Petrophysical Characterization of Unconventional Shale-Gas Reservoirs. In Proceedings of the International Oil and Gas Conference and Exhibition in China, Beijing, China, 8–10 June 2010.
110. Odusina, E.; Sondergeld, C.; Rai, C. An NMR Study on Shale Wettability. In Proceedings of the Canadian Unconventional Resources Conference, Alberta, Canada, 15–17 November 2011.
111. Sulucarnain, I.; Sondergeld, C.; Rai, C. *An NMR Study of Shale Wettability and Effective Surface Relaxivity*; Society of Petroleum Engineers: Richardson, TX, USA, 2012.
112. Borysenko, A.; Clennell, B.; Sedev, R.; Burgar, I.; Ralston, J.; Raven, M.; Dewhurst, D.; Liu, K. Experimental investigations of the wettability of clays and shales. *J. Geophys. Res. Solid Earth* **2009**, *114*, B07202. [CrossRef]
113. Dehghanpour, H.; Zubair, H.; Chhabra, A.; Ullah, A. Liquid Intake of Organic Shales. *Energy Fuels* **2012**, *26*, 5750–5758. [CrossRef]
114. Korb, J.; Nicot, B.; Louis-Joseph, A.; Bubici, S.; Ferrante, G. Dynamics and Wettability of Oil and Water in Oil Shales. *J. Phusical Chem.* **2014**, *118*, 23212–23218. [CrossRef]
115. Zolfaghari, A.; Dehghanpour, H.; Holyk, J. Water sorption behaviour of gas shales: I. Role of clays. *Int. J. Coal Geol.* **2017**, *179*, 130–138. [CrossRef]
116. Seemann, T.; Bertier, P.; Krooß, B.; Stanjek, H. Water vapour sorption on mudrocks. *Geol. Soc. Spec. Publ.* **2017**, *454*, 201–233. [CrossRef]
117. Charrière, D.; Behra, P. Water sorption on coals. *J. Colloid Interface Sci.* **2010**, *344*, 460–467. [CrossRef] [PubMed]
118. Hu, Y.; Devegowda, D.; Striolo, A.; Phan, A.; Ho, T.; Civan, F.; Sigal, R. Microscopic Dynamics of Water and Hydrocarbon in Shale-Kerogen Pores of Potentially Mixed Wettability. *SPE J.* **2015**, *20*, 112–124. [CrossRef]
119. Hu, Y.; Devegowda, D.; Sigal, R. A microscopic characterization of wettability in shale kerogen with varying maturity levels. *J. Nat. Gas Sci. Eng.* **2016**, *33*, 1078–1086. [CrossRef]
120. Kuila, U.; McCarty, D.; Derkowski, A.; Fischer, T.; Topor, T.; Prasad, M. Nano-scale texture and porosity of organic matter and clay minerals in organic-rich mudrocks. *Fuel* **2014**, *135*, 359–373. [CrossRef]
121. Gu, X.; Mildner, D.; Cole, D.; Rother, G.; Slingerland, R.; Brantley, S. Quantification of Organic Porosity and Water Accessibility in Marcellus Shale Using Neutron Scattering. *Energy Fuels* **2016**, *30*, 4438–4449. [CrossRef]
122. Li, J.; Wang, S.; Lu, S.; Zhang, P.; Cai, J.; Zhao, J.; Li, W. Microdistribution and mobility of water in gas shale: A theoretical and experimental study. *Mar. Pet. Geol.* **2019**, *102*, 496–507. [CrossRef]
123. Gao, Z.; Fan, Y.; Hu, Q.; Jiang, Z.; Cheng, Y.; Xuan, Q. A review of shale wettability characterization using spontaneous imbibition experiments. *Mar. Pet. Geol.* **2019**, *109*, 330–338. [CrossRef]
124. Shao, D.; Zhang, L.; Zhang, Y.; Zhang, Y.; Luo, H.; Qiao, B.; Yan, J.; Zhang, T. Water absorption characteristics of organic-rich shale of the Lower Cambrian in the Middle and Upper Yangtze region and its implications for shale gas exploration. *Nat. Gas Geosci.* **2020**, *31*, 1004–1015. (In Chinese with English abstract)
125. Sun, J. *Gas Bearing Properties and Controlling Factors of Shallow Longmaxi Shale in Northern Guizhou*; Guangzhou Institute of Geochemistry, Chinese Academy of Sciences: Beijing, China, 2020. (In Chinese with English abstract)
126. Bekyarova, E.; Hanzawa, Y.; Kaneko, K.; Silvestre-Albero, J.; Sepulveda-Escribano, A.; Rodriguez-Reinoso, F.; Kasuya, D.; Yudasaka, M.; Iijima, S. Cluster-mediated filling of water vapor in intratube and interstitial nanospaces of single-wall carbon nanohorns. *Chem. Phys. Lett.* **2002**, *366*, 463–468. [CrossRef]
127. Bahadur, J.; Contescu, C.; Rai, D.; Gallego, N.; Melnichenko, Y. Clustering of water molecules in ultramicroporous carbon: In-situ small-angle neutron scattering. *Carbon* **2017**, *111*, 681–688. [CrossRef]

128. Mamontov, E.; Yue, Y.; Bahadur, J.; Guo, J.; Contescu, C.; Gallego, N.; Melnichenko, Y. Hydration level dependence of the microscopic dynamics of water adsorbed in ultramicroporous carbon. *Carbon* **2017**, *111*, 705–712. [CrossRef]
129. Wu, Y.; Fan, T.; Jiang, S.; Yang, X.; Ding, H.; Meng, M.; Wei, D. Methane Adsorption Capacities of the Lower Paleozoic Marine Shales in the Yangtze Platform, South China. *Fuels* **2015**, *29*, 4160–4167. [CrossRef]
130. Shabani, M.; Moallemi, S.; Krooss, B.; Amann-Hildenbrand, A.; Zamani-Pozveh, Z.; Ghalavand, H.; Littke, R. Methane sorption and storage characteristics of organic-rich carbonaceous rocks, Lurestan province, southwest Iran. *Int. J. Coal Geol.* **2018**, *186*, 51–64. [CrossRef]
131. Tan, J.; Weniger, P.; Krooss, B.; Merkel, A.; Horsfield, B.; Zhang, J.; Boreham, C.; van Graas, G.; Tocher, B. Shale gas potential of the major marine shale formations in the Upper Yangtze Platform, South China, Part II: Methane sorption capacity. *Fuel* **2014**, *129*, 204–218. [CrossRef]
132. Ma, J.; Cai, Y.; Hu, Z.; Lu, C.; Wang, W. Water content in coal measure shale of Taiyuan Formation in Yushe Block, Qinshui Basin and its influence on pore characteristics. *Nat. Gas Geosci.* **2021**, *32*, 145–154. (In Chinese with English abstract)
133. Gao, P.; Xiao, X.; Hu, D.; Liu, R.; Cai, Y.; Yuan, T.; Meng, G. Water Distribution in the Ultra-Deep Shale of the Wufeng–Longmaxi Formations from the Sichuan Basin. *Energies* **2022**, *15*, 2215. [CrossRef]
134. Tong, J.; Han, X.; Wang, S.; Jiang, X. Evaluation of Structural Characteristics of Huadian Oil Shale Kerogen Using Direct Techniques (Solid-State C-13 NMR, XPS, FT-IR, and XRD). *Energy Fuels* **2011**, *25*, 4006–4013. [CrossRef]
135. Billemont, P.; Benoit, C.; Weireld, G. Adsorption of carbon dioxide, methane, and their mixtures in porous carbons: Effect of surface chemistry, water content, and pore disorder. *Langmuir* **2013**, *29*, 3328–3338. [CrossRef]
136. Wei, L.; Mastalerz, M.; Schimmelmann, A.; Chen, Y. Influence of Soxhlet-extractable bitumen and oil on porosity in thermally maturing organic-rich shales. *Int. J. Coal Geol.* **2014**, *132*, 38–50. [CrossRef]
137. Lan, Q.; Xu, M.; Binazadeh, M.; Dehghanpour, H.; Wood, J. A comparative investigation of shale wettability: The significance of pore connectivity. *J. Nat. Gas Sci. Eng.* **2015**, *27*, 1174–1188. [CrossRef]
138. Vandenbroucke, M.; Largeau, C. Kerogen origin, evolution and structure. *Org. Geochem.* **2007**, *38*, 719–833. [CrossRef]
139. Glorioso, J.; Rattia, A. *Unconventional Reservoirs: Basic Petrophysical Concepts for Shale Gas*; European Association of Geoscientists & Engineers: Vienna, Austria, 2012.
140. Bai, J.; Kang, Y.; Chen, M.; Chen, Z.; You, L. Impact of the water adsorption monolayer on methane ad-/desorption behavior in gas shale nanopores. *Ind. Eng. Chem. Res.* **2021**, *60*, 3130–3141. [CrossRef]
141. Li, P. *Wettability of Shale and its Control Mechanism for Methane Adsorption*; China University of Geosciences: Beijing, China, 2021. (In Chinese with English abstract)
142. Arnold, B.; Aplan, F. The hydrophobicity of coal macerals. *Fuel* **1989**, *68*, 651–658. [CrossRef]
143. Xv, M.; Bai, Y.; Xia, J. Discussion on Heterogeneous Wettability of Coal and Rock and Its Influencing Factors. In Proceedings of the Sixth National Natural Gas Reservoir Efficient Development Technology Seminar, Beijing, China, 11–14 May 2015; pp. 395–401+429. (In Chinese with English abstract)
144. Larsen, J.; Aida, M. Kerogen Chemistry 1. Sorption of Water by Type II Kerogens at Room Temperature. *Energy Fuels* **2004**, *18*, 1603–1604. [CrossRef]
145. Do, D.; Junpirom, S.; Do, H. A new adsorption–desorption model for water adsorption in activated carbon. *Carbon* **2009**, *47*, 1466–1473. [CrossRef]
146. Ungerer, P. State of the art of research in kinetic modelling of oil formation and expulsion. *Org. Geochem.* **1990**, *16*, 1–25. [CrossRef]
147. Li, J. *Study on the Occurrence Mode and Production Mechanism of Shale Gas*; China University of Petroleum: Beijing, China, 2017. (In Chinese with English abstract)
148. Xiang, J.; Zeng, F.; Liang, H.; Li, B.; Song, X. Molecular simulation of $CH_4/CO_2/H_2O$ adsorption in coal molecular structure. *Sci. China Earth Sci.* **2014**, *44*, 1418–1428. (In Chinese with English abstract)
149. Xia, Y.; Liu, X.; Liu, S. Adsorption mechanism of water molecules by oxygen-containing functional groups on lignite surface. *Coal Conversion.* **2016**, *39*, 9. (In Chinese with English abstract)
150. Tissot, P.B.; Welte, H.D. *Petroleum Formation and Occurrence*; Springer: Berlin, Germany, 1984; p. 699.
151. Helgeson, H.; Richard, L.; McKenzie, W.; Norton, D.; Schmitt, A. A chemical and thermodynamic model of oil generation in hydrocarbon source rocks. *Geochim. Cosmochim. Acta* **2009**, *73*, 594–695. [CrossRef]
152. Heuchel, M.; Davies, G.; Buss, E.; Seaton, N. Adsorption of Carbon Dioxide and Methane and Their Mixtures on an Activated Carbon: Simulation and Experiment. *Langmuir* **1999**, *15*, 8695–8705. [CrossRef]
153. Guo, J.; Zou, Y.; Yang, Y.; Qv, Z.; Wang, X.; Cai, Y.; Peng, P. Evolution characteristics of kerogen molecular structure in low maturity stage: Based on infrared spectrum analysis. *Geochimica* **2014**, *43*, 529–537. (In Chinese with English abstract)
154. Yang, C.; Xiong, Y.; Zhang, J. Differences in the development of hydrocarbon-generating organic pores in shale of different sedimentary types in China. *Geochemistry* **2019**, *48*, 544–554. (In Chinese with English abstract)
155. Zhao, Y.; Gao, P.; Zhou, Q.; Xiao, X.; Xing, Y.; Liu, W. A Review of the Heterogeneity of Organic-Matter-Hosted Pores in Shale Reservoirs. *Energies* **2022**, *15*, 8805. [CrossRef]
156. Cheng, P.; Xiao, X.; Wang, X.; Sun, J.; Wei, Q. Evolution of water content in organic-rich shales with increasing maturity and its controlling factors: Implications from a pyrolysis experiment on a water-saturated shale core sample. *Mar. Pet. Geol.* **2019**, *109*, 291–303. [CrossRef]

157. Gensterblum, Y.; Ghanizadeh, A.; Cuss, R.; Amann-Hildenbrand, A.; Krooss, B.; Clarkson, C.; Harrington, J.; Zoback, M. Gas transport and storage capacity in shale gas reservoirs—A review. Part A: Transport processes. *J. Unconv. Oil Gas Resour.* **2015**, *12*, 87–122. [CrossRef]
158. Liu, H.; Wang, G.; Fang, C.; Guo, W.; Sun, S. The formation mechanism of over pressure reservoir and target screening index of the marine shale in the South China. *Earth Sci. Front.* **2016**, *23*, 48–54.
159. Srodon, J.; Clauer, N.; Huff, W.; Dudek, T.; Banas, M. K-Ar dating of the Lower Palaeozoic K-bentonites from the Baltic Basin and the Baltic Shield: Implications for the role of temperature and time in the illitization of smectite. *Clay Miner.* **2009**, *44*, 361–387. [CrossRef]
160. Goulty, N.; Sargent, C.; Andras, P.; Aplin, A. Compaction of diagenetically altered mudstones—Part 1: Mechanical and chemical contributions. *Mar. Pet. Geol.* **2016**, *77*, 703–713. [CrossRef]
161. Ola, P.; Aidi, A.; Bankole, O. Clay mineral diagenesis and source rock assessment in the Bornu Basin, Nigeria: Implications for thermal maturity and source rock potential. *Mar. Pet. Geol.* **2018**, *89*, 653–664. [CrossRef]
162. Wang, Y.; Zhang, S.; Zhu, R. Water consumption in hydrocarbon generation and its significance to reservoir formation. *Pet. Explor. Dev.* **2013**, *40*, 259–267. [CrossRef]
163. Lahann, R. Impact of smectite diagenesis on compaction modeling and compaction equilibrium. *AAPG Memoir.* **2004**, *76*, 61–72.
164. Begum, M.; Yassin, M.; Dehghanpour, H. Effect of kerogen maturity on organic shale wettability: A Duvernay case study. *Mar. Pet. Geol.* **2019**, *110*, 483–496. [CrossRef]
165. Jagadisan, A.; Heidari, Z. Experimental Quantification of the Effect of Thermal Maturity of Kerogen on Its Wettability. *SPE Reserv. Eval. Eng.* **2019**, *22*, 1323–1333. [CrossRef]
166. Jagadisan, A.; Heidari, Z. Molecular dynamic simulation of the impact of thermal maturity and reservoir temperature on the contact angle and wettability of kerogen. *Fuel* **2022**, *309*, 122039. [CrossRef]
167. Yang, A.; Firdaus, G.; Heidari, Z. Electrical resistivity and chemical properties of kerogen isolated from organic-rich mudrocks. *Geophysics* **2016**, *81*, D643–D655. [CrossRef]
168. Jagadisan, A.; Heidari, Z. Application of X-Ray Photoelectron Spectroscopy in Connecting Thermal Maturity of Kerogen to Its Dielectric Constant in Organic-Rich mudrocks. In Proceedings of the SPWLA 58th Annual Logging Symposium, Oklahoma City, OK, USA, 17–21 June 2017.
169. Valdes, C.; Heidari, Z.; Gonzalez, A. Quantifying the Impacts of Thermal Maturity on Elastic Properties of Kerogen. In Proceedings of the SPWLA 58th Annual Logging Symposium, Oklahoma City, OK, USA, 17–21 June 2017.
170. Kozbial, A.; Li, Z.; Sun, J.; Gong, X.; Zhou, F.; Wang, Y.; Xu, H.; Liu, H.; Li, L. Understanding the intrinsic water wettability of graphite. *Carbon* **2014**, *74*, 218–225. [CrossRef]
171. Wei, Y.; Jia, C. Intrinsic wettability of graphitic carbon. *Carbon* **2015**, *87*, 10–17. [CrossRef]
172. Chen, J.; Gai, H.; Xiao, Q. Effects of composition and temperature on water sorption in overmature Wufeng-Longmaxi shales. *Int. J. Coal Geol.* **2021**, *234*, 103673. [CrossRef]
173. Curtis, M.; Cardott, B.; Sondergeld, C. Development of organic porosity in the Woodford Shale with increasing thermal maturity. *Int. J. Coal Geol.* **2012**, *103*, 26–31. [CrossRef]
174. Chen, J.; Xiao, X. Evolution of nanoporosity in organic-rich shales during thermal maturation. *Fuel* **2014**, *129*, 173–181. [CrossRef]
175. Cao, T.; Song, Z.; Wang, S.; Xia, J. Comparative study on specific surface area and pore structure of different shales and kerogen. *Sci. China* **2015**, *45*, 139–151. (In Chinese with English abstract) [CrossRef]
176. Powers, M. Fluid-release mechanisms in compacting marine mudrocks and their importance in oil exploration. *AAPG Bull.* **1967**, *51*, 1240–1254.
177. Gensterblum, Y.; Busch, A.; Krooss, B. Molecular concept and experimental evidence of competitive adsorption of H_2O, CO_2 and CH_4 on organic material. *Fuel* **2014**, *115*, 581–588. [CrossRef]
178. Huang, L.; Ning, Z.; Wang, Q.; Qi, R.; Zeng, Y.; Qin, H.; Ye, H.; Zhang, W. Molecular simulation of adsorption behaviors of methane, carbon dioxide and their mixtures on kerogen: Effect of kerogen maturity and moisture content. *Fuel* **2018**, *211*, 159–172. [CrossRef]
179. Sui, H.; Zhang, F.; Wang, Z.; Wang, D.; Wang, Y. Effect of Kerogen Maturity, Water Content for Carbon Dioxide, Methane, and Their Mixture Adsorption and Diffusion in Kerogen: A Computational Investigation. *Langmuir ACS J. Surf. Colloids* **2020**, *36*, 9756–9769. [CrossRef] [PubMed]
180. Sondergeld, C.; Newsham, K.; Comisky, J.; Rice, M.; Rai, C. Petrophysical Considerations in Evaluating and Producing Shale Gas Resources. In Proceedings of the SPE Unconventional Gas Conference, Pittsburgh, PA, USA, 23–25 February 2010.
181. Lahn, L.; Bertier, P.; Seemann, T.; Stanjek, H. Distribution of sorbed water in the pore network of mudstones assessed from physisorption measurements. *Microporous Mesoporous Mater.* **2020**, *295*, 109902. [CrossRef]
182. Zhang, Y. *Study on the Influence of Water-Bearing on Shale Gas Adsorption*; China University of Petroleum: Beijing, China, 2017. (In Chinese with English abstract)
183. Sun, J.; Xiao, X.; Wei, Q.; Cheng, P.; Tian, H.; Wu, Y. Gas in place and its controlling factors of the shallow Longmaxi shale in the Xishui area, Guizhou, China. *J. Nat. Gas Sci. Eng.* **2020**, *77*, 103272. [CrossRef]
184. Jagadisan, A.; Heidari, Z. Impacts of competitive water adsorption of kerogen and clay minerals on wettability of organic-rich mudrocks. *SPE Reserv. Eval. Eng.* **2020**, *23*, 1180–1189. [CrossRef]

185. Bi, H.; Jiang, Z.; Li, P.; Cheng, L.; Zeng, C.; Xv, Y.; Zhang, Y. Adsorption characteristics and influencing factors of Longmaxi Formation shale in southeast Chongqing. *Nat. Gas Geosci.* **2014**, *25*, 302–310. (In Chinese with English abstract)
186. Li, P.; Zhang, J.; Rezaee, R.; Dang, W.; Li, X.; Fauziah, C.; Nie, H.; TANG, X. Effects of swelling-clay and surface roughness on the wettability of transitional shale. *J. Pet. Sci. Eng.* **2021**, *196*, 108007. [CrossRef]
187. Zhang, M.; Fu, X. Study of the Characteristics of Marine-Terrigenous Facies Shale from the Permo-Carboniferous System in the Guxian Block, Southwest Qinshui Basin. *Energy Fuels* **2018**, *32*, 1096–1109. [CrossRef]
188. He, Q.; Dong, T.; He, S.; Zhai, G. Methane adsorption capacity of marine-continental transitional facies shales: The case study of the Upper Permian Longtan Formation, northern Guizhou Province, Southwest China. *J. Pet. Sci. Eng.* **2019**, *183*, 106406. [CrossRef]
189. Tabrizy, V.; Denoye, R.; Hamouda, A. Characterization of wettability alteration of calcite, quartz and kaolinite: Surface energy analysis. *Colloids Surf. A Physicochem. Eng. Asp.* **2011**, *384*, 98–108. [CrossRef]
190. Chen, Z.; Song, Y.; Li, Z.; Liu, S.; Li, Y.; Liu, G.; Yang, W.; Wang, Q.; Yang, Y.; Gao, F. The occurrence characteristics and removal mechanism of residual water in marine shales: A case study of Wufeng-Longmaxi shale in Changning-Weiyuan area, Sichuan basin. *Fuel* **2019**, *253*, 1056–1070. [CrossRef]
191. Wu, Q.; Deng, Y.; Fan, X.; Lu, H.; Wang, X.; Gang, Z.; Wang, F. Effect of Mineral Surface Properties on Water Behaviors in Pores Constructed by Calcite and Silica Particles. *J. Phys. Chem. C* **2019**, *123*, 13288–13294. [CrossRef]
192. Chai, R.; Liu, Y.; Wang, J.; Xin, J.; Pi, J.; Li, C. Molecular dynamics simulation of wettability of calcite and dolomite. *Jisuan Wuli/Chin. J. Comput. Phys.* **2019**, *36*, 474–482.
193. Wu, C.; Xue, H.; Lu, S.; Tian, S. Measurement and discussion of oil-water-mineral contact Angle for several common minerals. *Geoscience* **2018**, *32*, 842–849. (In Chinese with English abstract)
194. Li, J.; Chen, Z.; Li, X.; Wang, X.; Wu, K.; Feng, D.; QV, S. Quantitative study of liquid water distribution in shale and clay nano-pores. *Sci. China Technol. Sci.* **2018**, *48*, 1219–1233. (In Chinese with English abstract)
195. Sun, J.; Xiao, X.; Cheng, P. Influence of water on shale pore heterogeneity and the implications for shale gas-bearing property—A case study of marine Longmaxi Formation shale in northern Guizhou. *Mar. Pet. Geol.* **2021**, *134*, 105379. [CrossRef]
196. Ruppert, L.; Sakurovs, R.; Blach, T.; He, L.; Melnichenko, Y.; Mildner, D.; Alcantar-Lopez, L. A USANS/SANS Study of the Accessibility of Pores in the Barnett Shale to Methane and Water. *Energy Fuels* **2013**, *27*, 772–779. [CrossRef]
197. Li, H.; Guo, H.; Li, H.; Liu, W.; Jiang, B.; Hua, J. Thickness analysis of bound water film in tight reservoir. *Nat. Gas Geosci.* **2015**, *26*, 186–192.
198. Pan, L.; Xiao, X.; Tian, H.; Zhou, Q.; Chen, J.; Li, T.; Wei, Q. A preliminary study on the characterization and controlling factors of porosity and pore structure of the Permian shales in Lower Yangtze region, Eastern China. *Int. J. Coal Geol.* **2015**, *146*, 68–78. [CrossRef]
199. Chen, L.; Jiang, Z.; Liu, Q.; Jiang, S.; Liu, K.; Tan, J.; Gao, F. Mechanism of shale gas occurrence: Insights from comparative study on pore structures of marine and lacustrine shales. *Mar. Pet. Geol.* **2019**, *104*, 200–216. [CrossRef]
200. Zhou, S.; Zhang, D.; Wang, H.; Li, X. A modified BET equation to investigate supercritical methane adsorption mechanisms in shale. *Mar. Pet. Geol.* **2019**, *105*, 284–292. [CrossRef]
201. Yang, R.; Hu, Q.; Yi, J.; Zhang, B.; He, S.; Guo, X.; Hou, Y.; Dong, T. The effects of mineral composition, TOC content and pore structure on spontaneous imbibition in Lower Jurassic Dongyuemiao shale reservoirs. *Mar. Pet. Geol.* **2019**, *109*, 268–278. [CrossRef]
202. Li, A.; Han, W.; Fang, Q.; Memon, A.; Ma, M. Experimental investigation of methane adsorption and desorption in water-bearing shale. *Capillarity* **2020**, *3*, 45–55. [CrossRef]
203. Huang, H.; Li, R.; Lyu, Z.; Cheng, Y.; Zhao, B.; Jiang, Z.; Zhang, Y.; Xiong, F. Comparative study of methane adsorption of Middle-Upper Ordovician marine shales in the western Ordos Basin, NW China: Insights into impacts of moisture on thermodynamics and kinetics of adsorption. *Chem. Eng. J.* **2022**, *446*, 137411. [CrossRef]
204. Zou, J.; Rezaee, R.; Xie, Q.; You, L. Characterization of the combined effect of high temperature and moisture on methane adsorption in shale gas reservoirs. *J. Pet. Sci. Eng.* **2019**, *182*, 106353. [CrossRef]
205. Li, J.; Li, X.; Wu, K.; Feng, D.; Zhang, T.; Zhang, Y. Thickness and stability of water film confined inside nanoslits and nanocapillaries of shale and clay. *Int. J. Coal Geol.* **2017**, *179*, 253–268. [CrossRef]
206. Long, S.; Feng, D.; Li, F.; Du, W. Prospect analysis of the deep marine shale gas exploration and development in the Sichuan Basin, China. *J. Nat. Gas Geosci.* **2022**, *3*, 181–189. [CrossRef]
207. Guo, X.; Hu, D.; Huang, R.; Wei, Z.; Duan, J.; Wei, X.; Fan, X.; Miao, Z. Deep and ultra-deep natural gas exploration in the Sichuan Basin: Progress and prospect. *Nat. Gas Ind. B* **2020**, *7*, 419–432. [CrossRef]
208. Ma, X.; Wang, H.; Zhou, S.; Shi, Z.; Zhang, L. Deep shale gas in China: Geological characteristics and development strategies. *Energy Rep.* **2021**, *7*, 1903–1914. [CrossRef]